Sustainable Energy & Fuels

ROYAL SOCIETY OF CHEMISTRY

REVIEW

View Article Online
View Journal | View Issue

Cite this: *Sustainable Energy Fuels*, 2021, **5**, 5946

Progress on continuum modeling of lithium–sulfur batteries

Caitlin D. Parke, †[a] Linnette Teo, †[a] Daniel T. Schwartz *[a] and Venkat R. Subramanian *[b]

While lithium–sulfur batteries are a promising next-generation chemistry devices due to their high theoretical energy density, commercialization has been slow due to low coulombic efficiency and poor cycle life. This review explores the ways in which continuum modeling contributes to the understanding of lithium–sulfur (LiS) battery mechanisms and cell-level performance through the lens of micro- and macroscale phenomena. We examine different approaches to modeling important physical phenomena such as reaction mechanisms, cathode microstructure, shuttling, nucleation and precipitation, and transport limitations. This paper also emphasizes the significance and challenge of connecting typical modeling parameters and assumptions to systems-level metrics of a standard state-of-art high performing lithium–sulfur cell. Particularly important, the considerations for high energy density cells and the areas where continuum models can facilitate better collaboration are discussed. We also summarize a few selected works to highlight experimentally-driven modeling, use of electroanalytical techniques, and parameter identification approaches to enable model-based design and advanced battery management systems.

Received 16th July 2021
Accepted 28th October 2021

DOI: 10.1039/d1se01090e

rsc.li/sustainable-energy

Introduction

Research on lithium–sulfur (LiS) batteries has increased as electric transportation scales up, with a push for higher energy density chemistries and elimination of costly, low abundance, or insecure commodity materials from the battery supply chain. Lithium–sulfur batteries are projected to have about 3 times the energy density of lithium-ion batteries. Sulfur as a cathode material is cheap and abundant, two important considerations for both cost and supply chain availability.[1] Despite their promise, many challenges have slowed the commercialization of these batteries. Development of the lithium anode has been fraught with safety concerns and poor capacity retention.[2] During cycling, the sulfur cathode produces soluble polysulfide species that can travel to the anode and participate in deleterious side reactions, called polysulfide shuttling.[3] Efforts to control speciation and mitigate this parasitic shuttle

[a]*Department of Chemical Engineering, University of Washington, Seattle, Washington 98195, USA. E-mail: dts@uw.edu*

[b]*Walker Department of Mechanical Engineering & Material Science Engineering, Texas Materials Institute, The University of Texas at Austin, Austin, Texas 78712, USA. E-mail: venkat.subramanian@utexas.edu*

† These authors contributed equally to this work.

Dr Caitlin D. Parke is a current post-doctoral scholar at the University of Maryland. She received her PhD in Chemical Engineering from the University of Washington in 2021 and BSc in Chemical Engineering from the Ohio State University in 2015. Her research interests include physics-based modeling of next-generation lithium-based batteries, reduced-order models, and applications of machine learning to electrochemical systems.

Linnette Teo received her BSc in Chemical Engineering from Cornell University in 2017 and is currently a Chemical Engineering PhD candidate at the University of Washington, Seattle. She is also a Clean Energy Institute Graduate Fellow and is part of the DIRECT data science traineeship program. Her research focuses on physics-based modeling of diagnostics and electroanalytical techniques for advanced batteries.

	PHYSICAL SCALE			
MODELS	Atomistic simulations (AIMD, DFT, KMC)	Continuum modeling		Systems/stack level modeling
		Microscale (microkinetics/ particle level)	Macroscale (device level/ whole cell)	
EXPERIMENTS	Spectroscopic techniques	Electroanalytical techniques (CV, GITT/PITT, EIS), surface microscopy	Cycling, EIS, resistance measurements	Cycling, thermal measurements
APPLICATIONS	Discovery and design of new cathode material and solvent	Identification of physical constants, speciation, underlying mechanisms	Design and optimization of whole cell performance	BMS monitoring and control, cell/module/pack management

Fig. 1 A spectrum of modeling scales that can inform and be validated by different types of experiments for various applications in the lithium–sulfur field.

phenomena have focused both on electrolyte engineering and protection of the lithium anode.[1,4] Additionally, the sulfur solid species within the cathode are insulating, which can lead to passivation and overall poor sulfur utilization.[5] To mitigate this, carbon and other additives are included to improve conductivity, but which decreases overall energy density. Work on nano-structured cathodes that can anchor polysulfide species to the surface have been developed to overcome this. Carbon-to-sulfur (C/S) and electrolyte-to-sulfur (E/S) ratios are important metrics for development of practical high energy density cells as calculations show that "lean" cell conditions are vital to reach these goals.[6,7]

Modeling can be useful to accelerate the progress of lithium–sulfur battery development. Battery models span a wide range of scales from atomistic simulations on the angstrom scale all the way to packs of battery used in a vehicle on the scale of meters. The focus of this paper is on continuum modeling which lies in between these two extremes (see Fig. 1). We can further split continuum modeling into the microscale and macroscale. Taking traditional chemical engineering reaction kinetics as an analog, there are also two scales of modeling. Microkinetic modeling focuses on breaking down reactions to elementary steps with individual activation energies and species, whereas macroscale chemical reaction modeling takes the bulk reaction rate constants and rate limiting steps to design a chemical reactor where an engineer is concerned about flow rate and product yield. Similarly, we will structure this paper by describing continuum modeling of lithium–sulfur batteries using microscale and macroscale terminology. Microscale modeling is about representing key physical phenomena in a mechanistic manner to elucidate underlying mechanisms. Besides microkinetics, this can be looking at the cathode structure in greater morphological detail, modeling sub-micron level internal transport into a particle, or nucleation and growth

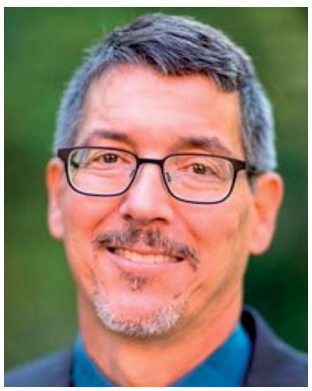

Daniel T. Schwartz is Boeing-Sutter Professor of Chemical Engineering and director of the University of Washington Clean Energy Institute. His electrochemical engineering research explores the performance of energy storage, conversion, and electrodeposition systems. A 2016 recipient of the Presidential Award for Excellence in Science, Mathematics and Engineering Mentoring from the White House, he is also a Fellow of the Electrochemical Society and member of the Washington State Academy of Sciences. He serves on State energy and climate policy committees, as an advisor to Chief Leschi Schools, and on the board and executive committee of the CleanTech Alliance.

Professor Venkat R. Subramanian received his B.Tech. degree in chemical and electrochemical engineering from the Central Electrochemical Research Institute (CECRI), Karaikudi, India, in 1997 and his Ph.D. degree in chemical engineering from the University of South Carolina, Columbia, SC, USA, in 2001. Professor Subramanian is an elected ECS Fellow and a past elected chair of IEEE division of the Electrochemical Society. He is also a past elected technical editor of the Electrochemical Society. His group aims to be the world's leading group in the areas of model-based Battery Management System and model-based design of current and next-generation energy storage devices.

of precipitates for example. This kind of modeling on the microscale can be aided by electroanalytical experiments (*e.g.*, cyclic voltammetry (CV), galvanostatic or potentiostatic intermittent titration techniques (GITT/PITT), electrochemical impedance spectroscopy (EIS)) to identify physical constants and speciation, specialized setups like rotating disc electrodes, or microscopy to probe surface and structure evolution. Macroscale modeling is on the scale of whole cell and device level and is focused on modeling effective properties to relate to overall cell performance such as voltage curves. Macroscale models are typically used to explore experimentally-relevant conditions by revealing how important cell parameters like thickness, porosity, and sulfur loading impact the internal states of the battery, such as the speciation, kinetics, and transport, without the time and cost of traditional experiments. Modeling can explore design space and optimize for multiple metrics at once, which can point experimentalists in a new direction.

Continuum modeling covers a broad range of possible applications and is an exciting field as it can tie in with the opposite two ends of the modeling spectrum. Atomistic simulations such as *ab initio* molecular dynamics (AIMD), density functional theory (DFT), and kinetic Monte Carlo (KMC) techniques can perform first principles calculations and simulations on fundamental interactions to determine molecular properties like surface and absorption energies, transport properties, or reaction pathways that can be used as a parameter to be varied in continuum modeling to aid solvent engineering, for example. On a systems/stack level, for applications like a battery management system (BMS) in a vehicle's battery pack, continuum models are used for monitoring and control, computationally efficient macroscale continuum models for a cell can be extended to more extensive module and pack level systems. In this review, we highlight the areas where continuum models have collaboratively improved understanding of lithium–sulfur batteries and touch on other areas where further model development is key.

In continuum modeling, the lithium–sulfur cell can be thought of as having three domains to be modeled as a cell sandwich – the lithium anode, porous separator, and composite cathode – as seen in Fig. 2. For a fully charged cell, the cathode starts off as a composite of solid S_8(s) and carbon particles with assumed uniform porosity (more complex cathode morphology will be discussed in the Cathode structure section). The solid sulfur dissolves and is electrochemically reduced through a series of cascading steps to lower order polysulfides. The 5-step reduction mechanism shown in Fig. 2 is a popular proposed scheme and simplifications/variations are discussed later. The higher order polysulfides are typically soluble in conventional electrolytes while the lower order polysulfides such as Li_2S and sometimes Li_2S_2 are insoluble products. Solid products such as Li_2S form as a film on the cathode and surface passivation of the carbon structure occurs towards the end of discharge. Shuttling also occurs which is when the dissolved polysulfides are transported back and forth between the two electrodes and can be reduced at both. A resulting phenomenon of shuttling is surface passivation at the anode which results in irreversible capacity loss. In this work, we will review papers that model cathode structure, nucleation and growth of solid products, shuttling, and degradation processes such as anode passivation. We will also relate models with experimental trends observed, and importantly, experimental design and metrics. For macroscale models to be deemed useful, simulated voltage discharge curves are typically compared to that of high-performance experimental cells, where the three key features are: two voltage plateaus and a voltage dip and recovery as a transition between the two plateaus (refer to Fig. 3b and 4 for examples). This dip, or negative differential resistance, is normally attributed to solid nucleation processes which we will describe further in the Precipitation section. This review will cover both lumped/zero-dimensional (0D) models, and one-dimensional (1D) models, where 1D models capture the spatial variation in each domain, and 0D models generally only model the cathode as a singular point. The typical equation set

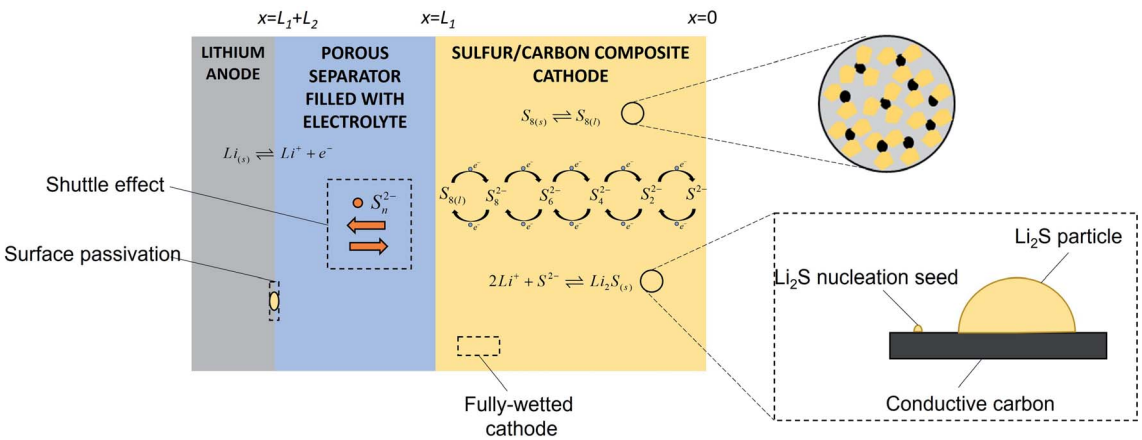

Fig. 2 Schematic of lithium–sulfur sandwich layer with lithium anode, porous separator, and composite cathode with yellow solid sulfur particles, black conductive carbon, and binder. The reaction scheme in the cathode is a commonly proposed formulation but is by no means the best formulation. Other processes that can occur is Li_2S film formation in the cathode through a nucleation and growth process, shuttling of polysulfides across the cell, and the resulting surface passivation at the anode.

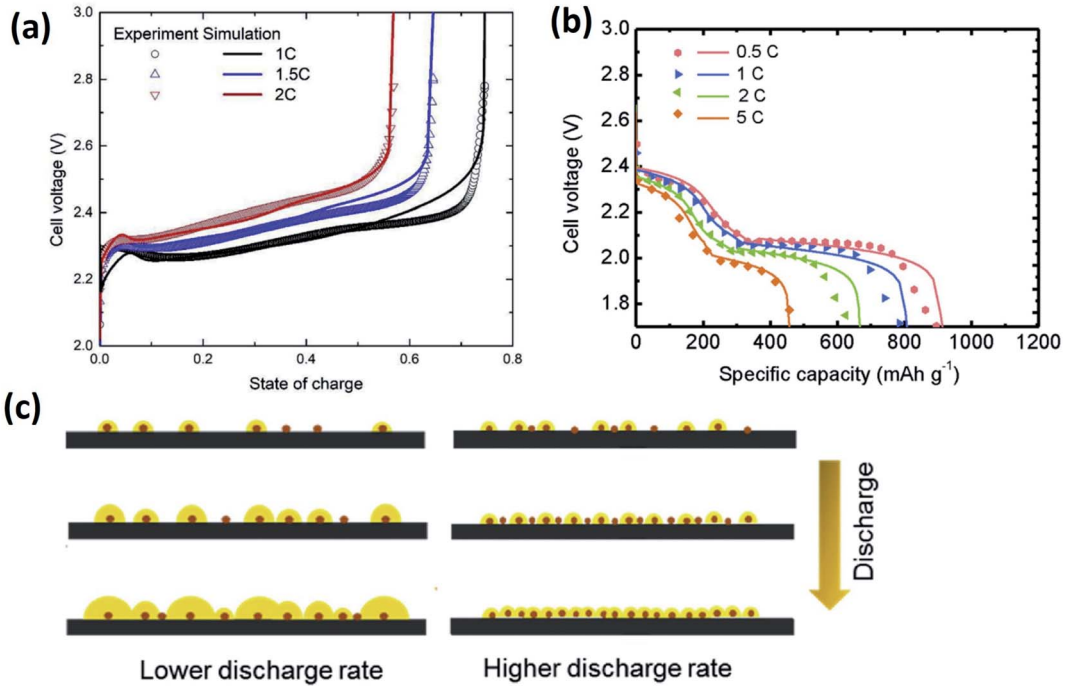

Fig. 3 Nucleation and growth models can reproduce the rate-dependent (a) charge and (b) discharge voltage curves. (c) For lower discharge rates, fewer Li_2S nuclei form, leading to more uneven distribution of and larger particle sizes; at higher discharge rates, the nucleation rate is higher and particle growth is more uniform. (a) is reprinted from ref. 37 with permission from *Electrochimica Acta*. (b) and (c) are reprinted from ref. 38 with permission from the *Journal of Power Sources*.

for the 1D model is shown in Table 1, which describes the thermodynamics, kinetics, and transport detailed by Kumaresan *et al.*[8] Included within Table 1 are degradative redox reactions from polysulfide shuttle, taken from Mistry and Mukherjee (detailed within Shuttling, degradation, and lithium anode dynamics).[9]

Cathode reaction scheme

There are two different commonly employed reduction schemes for the sulfur cathode. The first scheme employs the two reactions shown below.

$$S_{8(l)} + 4e^- \rightleftharpoons 2S_4^{2-} \quad (1)$$

$$S_4^{2-} + 4e^- \rightleftharpoons 2S^{2-} + S_2^{2-} \quad (2)$$

This simple reduction scheme was first shown in the work by Mikhaylik and Akridge in a lumped model.[10] Other lumped or simplified 1D models[11–13] employed the same reaction scheme but included chemical reactions of S_8 dissolution or precipitation of Li_2S. In general, the relatively simple reaction scheme is used for the express purpose of predicting trends and ease of parameterization. The voltage curve only qualitatively matches the relevant features, like the two plateaus and voltage dip. Work by Erisen *et al.*[13] concluded that modeling the first plateau with a single reaction does not adequately describe the behavior and that the presence of several long-chain polysulfides are needed to replicate the first plateau more quantitatively. Using this simple reduction scheme inadequately describes the complexity of the chemistry at play but can be very useful to understand trends due to the low computational footprint. This is an example of macroscale continuum modeling where deliberate approximations are made to simply match key experimental traits of a voltage curve.

On the other hand, microscale modeling aims to break down this reaction scheme to the most accurate representation. A more complex reduction scheme was proposed in the model by Kumaresan *et al.*[8] In contrast to the earlier work by Mikhaylik, the reaction scheme included a 5-step reduction of sulfur from dissolved S_8 to S^{2-}. This 5-step reduction is a step towards a more microscale understanding of the reaction scheme by breaking down the lumped steps further. The electrochemical reaction steps are shown in Fig. 2. For each of the charged polysulfides, the model includes precipitation of $Li_2S_n(s)$. Other models have tweaked this reaction scheme. For example, some models only consider $Li_2S(s)$ and occasionally $Li_2S_2(s)$ because there is still debate about the presence of other solid precipitates.[12,14,15]

This more complex reduction scheme is able to reproduce the important features of the discharge curve, but even so, it is a simplification of the complicated schemes that have been proposed, which include disproportionation and dissociation reactions with multiple pathways.[16–19] Elucidating the reaction scheme is an important step to identifying the underlying phenomena that contribute to performance limitations. We can go even further to the left of the microscale spectrum by using electroanalytical techniques and spectroscopic methods to

Table 1 Standard 1D equations for lithium–sulfur batteries, modified from ref. 8 with anode expressions from ref. 9

Governing equations	Boundary conditions
Positive electrode (region 1)	
$\frac{\partial \varepsilon_1 C_{1,i}}{\partial t} = -\frac{\partial N_{1,i}}{\partial x} + r_i - R_{1,i}$	$N_{1,i}\|_{x=0} = 0$
$N_{1,i} = -D_{1,i}\frac{\partial C_{1,i}}{\partial x} - z_i\frac{D_{1,i}}{RT}FC_{1,i}\frac{\partial \phi_{1,e}}{\partial x}$	$-\sigma\frac{\partial \phi_s}{\partial x}\Big\|_{x=0} = i_{app}$
$i_s = -\sigma\frac{\partial \phi_s}{\partial x}$	$i_{1,e}\|_{x=0} = 0$
$i_{1,e} = F\sum_i z_i N_{1,i}$	
$\frac{\partial \varepsilon_{1,k}}{\partial t} = \tilde{V}_k R_k'$	
$\frac{\partial \varepsilon_1}{\partial t} = \sum_k \tilde{V}_k R_k'$	
Separator (region 2)	
$\frac{\partial \varepsilon_2 C_{2,i}}{\partial t} = -\frac{\partial N_{2,i}}{\partial x} - R_{2,i}$	$C_{1,i}\|_{x=L_1} = C_{2,i}\|_{x=L_1}$
$N_{2,i} = -D_{2,i}\frac{\partial C_{2,i}}{\partial x} - z_i\frac{D_{2,i}}{RT}FC_{2,i}\frac{\partial \phi_{2,e}}{\partial x}$	$i_{1,e}\|_{x=L_1} = i_{2,e}\|_{x=L_1}$
$i_{2,e} = F\sum_i z_i N_{2,i}$	$N_{1,i}\|_{x=L_1} = N_{2,i}\|_{x=L_1}$
$\frac{\partial \varepsilon_{2,k}}{\partial t} = \tilde{V}_k R_k'$	$-\sigma\frac{\partial \phi_s}{\partial x}\Big\|_{x=L_1} = 0$
$\frac{\partial \varepsilon_2}{\partial t} = \sum_k \tilde{V}_k R_k'$	
Anode/separator interface with shuttle equations	
$i_{2,e}\big\|_{x=L_1+L_2} = F\sum_i z_i N_{2,i}$	$N_{2,Li^+}\big\|_{x=L_1+L_2} = \frac{i_{i,app}}{F} + r_i'$
$N_{2,i}\big\|_{x=L_1+L_2} = r_i'$	$\phi_s\|_{x=L_1+L_2} = 0$
$r_i' = \sum_j s_{i,j} k_j' \left(\frac{C_i}{C_i^{ref}}\right)^{s_{i,j}}$	$k_j' = \frac{i_{0,j}}{F}\exp\left(-\frac{F\eta}{2RT}\right)$
Other expressions	
$r_i = -a\sum_j \frac{s_{i,j} i_j}{n_j F}$	$a = a_0\left(\frac{\varepsilon}{\varepsilon_{initial}}\right)^{\xi}$
$\frac{\partial i_s}{\partial x} + \frac{\partial i_e}{\partial x} = 0$	$\frac{\partial i_e}{\partial x} = a\sum_j i_j$
$\eta_j = \phi_s - \phi_e - U_{j,ref}$	$U_{j,ref} = U_j^{\theta} - \frac{RT}{n_j F}\sum_i s_{ij}\ln\left[\frac{C_{i,ref}}{1000}\right]$
$R_i = \sum_k \gamma_{i,k} R_k'$	$R_k' = k_k \varepsilon_{1,k}\left(\prod_i C_{1,i}^{\gamma_{i,k}} - K_{sp,k}\right)$
$D_i = \varepsilon^{\xi} D_{i,0}$	$i_j = i_{0,j,ref}\left\{\left(\frac{C_{i,anodic}}{C_{i,ref}}\right)^{s_{a,j}}\exp\left(\frac{\alpha_{a,j}F}{RT}\eta_j\right) - \left(\frac{C_{i,cathodic}}{C_{i,ref}}\right)^{-s_{c,j}}\exp\left(-\frac{\alpha_{c,j}F}{RT}\eta_j\right)\right\}$

figure out detailed speciation. CV experiments give a wealth of information about the redox behavior of electrochemical systems, and some studies have combined CV experiments with modeling to analyze the reaction scheme.

Work by Schön and Krewer[20] coupled identification of species *via* high performance liquid chromatography and CV experiments and modeling to analyze two proposed reaction mechanisms. The electrolyte system consisted of 1 M LiTFSI and a 1 : 1 mixture of 1,3-dioxolan (DOL) : DME. The simplified reaction mechanism, originally proposed by Lu *et al.*,[21] is made of two electrochemical reactions and an irreversible chemical reaction (EEC); the sulfur species are left unidentified (written as X and Y) since it is empirically derived.

$$X \rightleftarrows \ldots \xrightleftharpoons{-5.4e^-} X^{5.4-} \quad (3)$$

$$X^{5.4-} \rightleftarrows \ldots \xrightleftharpoons{-2e^-} X^{7.4-} \quad (4)$$

$$X^{7.4-} \rightarrow \ldots \xrightarrow{+7.4Li^+} Y \quad (5)$$

When modeling CV with the EEC mechanism, the reduction and oxidation peaks are reproduced, but within the diffusion limited regime, the model predictions missed a second cathodic peak and exhibited a cathodic current not seen experimentally. The authors recommended using the EEC reduction scheme when the electrolyte composition is not

relevant, such as reproducing voltage trends. In order to match the variety of species seen in high performance liquid chromatography (HPLC), the other reaction mechanism (E3C4) included three electrochemical reactions and four chemical reactions with both dissociation and disproportionation.

$$S_8 + 2e^- \rightleftharpoons S_8^{2-} \quad (6)$$

$$S_8^{2-} + 2e^- \rightleftharpoons S_8^{4-} \quad (7)$$

$$S_4^{2-} + 2e^- \rightleftharpoons 2S_2^{2-} \quad (8)$$

$$S_8^{4-} \rightleftharpoons 2S_4^{2-} \quad (9)$$

$$3S_4^{2-} \rightleftharpoons S_8 + S_2^{2-} + 2S^{2-} \quad (10)$$

$$2S_3^{2-} \rightleftharpoons S_4^{2-} + S_2^{2-} \quad (11)$$

$$2S_2^{2-} \rightleftharpoons S_3^{2-} + S^{2-} \quad (12)$$

The E3C4 kinetic model is able to reproduce both kinetic and transport limited behavior shown in CV experiments. The authors noted that the redox behavior varies with both SOC and direction of the current, and the disproportionation reactions were necessary to reproduce a circular conversion of shorter polysulfides to $S_{8(l)}$. This work suggests that the oxidation and reduction behavior for charge and discharge is different, and to reproduce full-cell charging behavior it may be necessary to include more complex chemistry than previously modeled. The E3C4 kinetic model is well-suited to more detailed modeling of the interplay of the electrolyte system and the speciation on the cell limitations, such as polysulfide shuttle or surface passivation by sulfur precipitates.

Recent work by Thangavel *et al.*[22] studied the CV behavior of a three electrode cell with a planar glassy carbon working electrode in a tetraethylene glycol dimethyl ether:dioxolane (TEGDME:DOL) electrolyte with 1 M lithium bis(trifluoromethanesulfonyl)imide (LiTFSI) and with S_8, Li_2S_8, and Li_2S_6 as the starting electroactive species. With a 1D model of the working electrode and adjacent electrolyte diffusion layer, the model was unable to model all the features of the redox behavior with the standard 5-step reduction scheme described previously. After the addition of an alternative reaction pathway including $S_3^{\bullet-}$ and $S_2^{\bullet-}$ radical species, the CV results were successfully reproduced, and reasonable estimates for the new reaction parameters were obtained. The added pathway includes:

$$S_8^{2-} \rightleftharpoons 2S_4^{\bullet-} \quad (13)$$

$$S_4^{\bullet-} + e^- \rightleftharpoons S_4^{2-} \quad (14)$$

$$S_6^{2-} \rightleftharpoons 2S_3^{\bullet-} \quad (15)$$

The CV modeling represents a promising step forward in improving the proposed reaction scheme for lithium–sulfur batteries and extracting meaningful parameter values that can be further analyzed in a battery setup with sparse electrolyte amounts and high surface area electrodes.

Studies have shown that the speciation is dependent on the electrolyte system, additives, and solvent.[23] Here we highlight another example of macroscale modeling where reaction rates are adjusted to match experimentally observed cell voltage for a system with additives. Work by Shim *et al.*[24] combined experimental and modeling work to explore the effects of the $LiNO_3$ additive. $LiNO_3$ has been used to mitigate polysulfide shuttling by promoting a beneficial anode protective layer, thus preventing side reactions with polysulfides at the anode. However, $LiNO_3$ has been reported as negatively impacting the reduction of Li_2S_2 at the cathode and causing a distortion of the voltage curve and creating a third plateau. Their work found that the cells with high concentrations of $LiNO_3$ exhibited a third plateau. By controlling the exchange current density for the reduction of S_2^{2-} to S^{2-} and decreasing the reduction rate with excess $LiNO_3$ present, the model was able to reproduce the results seen experimentally. In the presence of excess $LiNO_3$, the model attributed the middle plateau to production of $Li_2S_2(s)$ and the third plateau as a further reduction to $Li_2S(s)$. The final two reduction reactions (S_4^{2-} to S_2^{2-} and S_2^{2-} to S^{2-}) usually occur simultaneously; with excess $LiNO_3$, the two reactions occur one at a time, causing the distinctive separation of the second plateau.

Electrolyte engineering is another important area of study as different electrolytes have been shown to stabilize different species and affect the reduction scheme. A simple experiment by the Manthiram group[25] mixed $Li_2S_6(s)$ with DOL : DME and 3 other promising electrolytes and measured the UV-vis spectra. Each of the electrolytes stabilized different species, including a commonly reported radical anion $S_3^{\bullet-}$. Parke *et al.*[26] explored the effects of the $S_3^{\bullet-}$ radical formation on the cell-level behavior of a battery for the first time. The reaction scheme in Fig. 2, an E5C2 mechanism, was modified by including an additional chemical dissociation step (eqn (15)) that formed $S_3^{\bullet-}$, creating a E5C3 model that matches experimentally observed speciation better. Both the thermodynamics and kinetics of radical anion formation was shown to have a dramatic effect on the voltage curve. With instantaneous kinetics, the low depth-of-discharge voltage actually increased while the rest of the curve was depressed compared to no $S_3^{\bullet-}$ chemistry. With slower kinetics, the dissociation reaction served as a sink of sulfur and resulted in reversible capacity loss. This work represents an important step in understanding the effects of electrolyte stabilization on the full-cell behavior and underlies the need for accurate thermodynamic and kinetic parameters. Such parameters could be obtained by using molecular simulations to study polysulfide stability.[27,28]

Reversibility of cathode for charging models

Most models have been able to simulate discharge voltage curves that match experimental features well. However, simulating charge curves using the same set of governing equations have proven to be challenging. Each of the electrochemical and precipitation reactions proposed in the Kumaresan model have reversible terms (see Table 1), which indicates that the model should be intrinsically reversible and be able to discharge and

charge. However, Ghaznavi and Chen[29] found that the Kumaresan model[8] was unable to charge due to a low saturation concentration of Li_2S. In a later paper, Ghaznavi and Chen[30] varied the solubility product of Li_2S, K_{sp,Li_2S}, and showed that increasing that by seven orders of magnitude, *i.e.*, a factor of 10^7, from the commonly assumed value of 9.95×10^{-4} mol^3 m^{-9}, allowed for charging to be simulated at a low 0.02C rate. There have been no reported values of experimentally measured K_{sp,Li_2S} beyond the assertion of it being highly insoluble. The range of values of K_{sp,Li_2S} used in the modeling literature[8,31] is large and range from 10^{-5} to 10^7 mol^3 m^{-9}. There is a need for careful measurement of precipitation related parameters in conventionally used electrolytes for more accurate models. Perhaps, atomistic-scale simulations, such as quantum chemistry calculations or MD,[32] can inform solubility and rate constants, at least to an order of magnitude range. Li_2S precipitation determines the S^{2-} concentration, hence shifting the reduction potential. This shift in reduction potential has been observed in GITT experiments[33] and Zhang *et al.*[34] suggested that GITT might be useful to estimate precipitation rate constants and solubility products.

In terms of capturing specific features of charging curves, Ghaznavi and Chen[30] compared their simulated charging voltage curves to experimental curves and reported inability of the model to reproduce the experimentally observed sharp voltage peak at the start of charge. Their simulated charging curve also has an additional peak in the middle of charging, that can be attributed to sulfur precipitation, but is not seen experimentally. Additionally, Kumaresan model's precipitation rate expression includes the solid volume fraction of the precipitate to account for the slow nucleation process at the start of precipitation. This has been reported to be numerically unstable for precipitation when the volume fractions are close to zero. Yoo *et al.*[35] introduced the addition of extra aphysical terms for the precipitation reactions of S_8 and Li_2S to overcome this challenge of numerical instability. Using the rate of change of the volume fraction of Li_2S, $\varepsilon_{Li_2S_{(s)}}$, as an example,

$$\frac{\partial \varepsilon_{Li_2S_{(s)}}}{\partial t} = V_{Li_2S_{(s)}}\left[k_{Li_2S_{(s),1}}\left(C_{Li^+}{}^2 C_{S^{2-}} - K_{sp,Li_2S}\right) + k_{Li_2S_{(s),2}}\frac{C_{Li^+}{}^2 C_{S^{2-}}}{\varepsilon_{Li_2S_{(s)}}}\right] \quad (16)$$

where V, k, C, are the molar volume, precipitation/dissolution rate constant, and concentration respectively, the first term on the right-hand side of eqn (16) describes the precipitation rate and is the same as in Table 1, while the second is the additional aphysical term. They were able to simulate a charging curve but were not able to capture all features well.

Better parameterization of the models mentioned above might solve some of the charging challenges and numerical instabilities observed. Another possibility might be due to the proposed models having inaccurate or missing mechanisms. This can be due to the limiting phenomena being mass transfer rather than charge transfer, for example. Zhang *et al.*[36] used a simple 0D model with transport-limited kinetics and was the first to demonstrate the voltage kink at the start of charge (more details about this model in Transport section). It is clear that macroscale modeling is unable to fully resolve the inconsistences in charging and a deeper dive into microscale mechanistic models is necessary.

On a microscale level, for example, missing mechanisms that might help solve the charging challenge are reactions and species that are unaccounted for such as the radical species $S_3^{\bullet-}$ highlighted by Parke[26] and the fact that dissolution/precipitation phenomena are not well captured in earlier models. As discussed earlier within the Cathode reaction scheme section, CV modeling by Schön and Krewer[20] indicated different redox behavior for charge and discharge, which was replicated only with additional chemical dissociation and disproportionation reactions providing parallel pathways. With the addition of nucleation and growth phenomena to describe the precipitation process, Xiong *et al.*[37] were able to replicate the charging curves well (see Fig. 3a) but they did not explore discharge. Danner *et al.*[31] explored both charging and discharging, but even with the addition of detailed nucleation and growth phenomena, were still unable to capture charging features well (discussed in more detail in Precipitation section). Having a comprehensive model that captures both discharge and charge features remains a major challenge. We recommend sustained efforts in developing more accurate and validated charging models, including thoughtful coordination of analytical, electroanalytical, and engineering approaches to determine trustworthy physicochemical parameters, so that continuum modeling may impact development of LiS batteries by both model-based design and performance optimization.

Precipitation phenomena in the cathode

In macroscale modeling, the voltage dip during discharge is usually described by having initially slow precipitation kinetics mimicking a nucleation overpotential where supersaturation occurs (see other expressions in Table 1). The precipitation rate is a function of the volume fraction of precipitate which is slow at first and as the volume fraction increases, so does the rate of precipitation. Therefore, precipitation phenomena is described macroscopically using a balance of the precipitation rate constant and solubility limit (as demonstrated in the Ghaznavi and Chen[30] parameter study mentioned in the Charging section).

This section will highlight papers that have focused on capturing the precipitation/dissolution phenomena with more detailed microscale models. Microscale continuum models that couple bulk transport and electrochemical kinetic processes with particle-level nucleation and growth theory might resolve some of the discrepancies seen between experiments and macroscale continuum models that model only model precipitation as a bulk process.

The first model to incorporate nucleation and growth to describe the precipitation reactions in a 1D lithium–sulfur model is by Ren *et al.*,[38] who modeled Li_2S precipitation as an electrochemical reaction between Li^+ and S_4^{2-} (eqn (17)) using

Tafel kinetics (eqn (18)), which is typically used for irreversible reactions:

$$\frac{4}{3}Li^+ + \frac{1}{6}S_4^{2-} + e^- \rightarrow \frac{2}{3}Li_2S \quad (17)$$

$$i_L = i_{0,L}(1-\theta)\exp\left(\frac{\alpha\eta_L F}{RT}\right) \quad (18)$$

where i_L is the current density describing the lower voltage plateau, $i_{0,L}$ is a rate constant, θ is the fraction of surface covered by Li_2S, α is the charge transfer coefficient, η_L is the overpotential, F is Faraday's constant, R is the molar gas constant, and T is temperature.

They specifically assumed Li_2S dissolution does not occur and hence there is no backward dissolution reaction modeled, rendering the model only applicable for discharge. In their model, the equation for nucleation rate is based on electrolytic nucleation of metals and considers overpotential for S_4^{2-} adsorption, where the nucleation rate, P, expressed as:

$$P = P_0\left(\tilde{C}_{Li^+}\right)^{\frac{4}{3}}\left(\tilde{C}_{S_4^{2-}}\right)^{\frac{1}{6}}(1-\theta)\exp\left(\frac{\alpha\eta_L F}{RT}\right) \quad (19)$$

where P_0 is the initial nucleation rate and $\tilde{C}$ are dimensionless concentrations. For the growth portion, Ren *et al.* assumed hemispherical particles, used Kolmogorov phase transformation theory to account for overlap, and presented expressions for surface coverage and radial growth rate. They were able to simulate discharge curves from 0.5C to 5C and show that both plateaus are shortened, and hence higher capacity loss is seen, with increased C-rate, as shown in Fig. 3b. In comparison with experimental data, average errors found are less than 3%. Additionally, they showed the distributions of Li_2S particle radius with C-rate (Fig. 3c). They found that at higher rates, larger overpotentials enable higher nuclei density, resulting in uniform morphology of small particles. At lower rates, growth of particles is the dominating process, which results in fewer but larger particles. This description of particle size matched SEM images of surface coverage. Analysis of the impact of initial nuclei density on specific capacity showed a non-monotonic trend, which indicates the need for optimization to balance between a high average particle size and a uniform particle distribution. By incorporating the relation between overpotential and surface coverage, Ren *et al.* was able to relate rate-dependent morphology of Li_2S precipitation to show rate-dependent capacity trends.

Similar to Ren *et al.*, Andrei *et al.*[39] used a standard set of multispecies cell-level charge and transport equations to describe the bulk and coupled that to nucleation and growth of polysulfide precipitates. They used classical nucleation theory to derive and relate the driving force of nucleation to oversaturation instead of using electrolytic nucleation that Ren *et al.* adopted. However, Andrei *et al.* demonstrated how both nucleation rate equations are mathematically similar. There were a few approximations made to reduce the number of fitting parameters and also a linear diffusive concentration gradient of polysulfides away from the carbon surface was assumed. To keep track of nuclei size distribution spatially across the cell, Andrei *et al.* used the differential form of Kolmogrov equation to describe surface coverage.

Upon qualitative comparison to experimental data, simulations by Andrei *et al.* were able to match the trend of discharge capacity decreasing with increasing rate for 0.1C to 1C. They were able to attribute this trend to cathode passivation due to solid products by showing surface coverage and number of Li_2S nuclei changing during discharge, with complete surface coverage occurring earlier for higher rates. They also explored supersaturation trends during discharge and advised for the use of an electrolyte that enables high solubility of intermediate polysulfides to prevent intermediate products from forming on the cathode surface and taking a long time to dissolve (though this might contribute to higher degradation from shuttling phenomena). Through a variable discharge rate experiment, they found that different dynamics of nuclei growth occur at different C-rates. Their simulations matched their experiment qualitatively, and they were able to ascribe the difference in rate of surface coverage to different starting points of nucleation.

The previous two models look at the impact of adding more detailed precipitation expressions to describe discharge, while Xiong *et al.*[37] focused on modeling the charging process. Their model introduced the concept of a redox mediation phenomenon during rate-dependent Li_2S dissolution based on experimental evidence.[16,40] They start with an assumption of a bimodal particle size distribution where small and large Li_2S particles are distributed evenly at the beginning of charge. Dissolution of the Li_2S particles is modeled as an electrochemical oxidation process to Li_2S_4, which is further oxidized to Li_2S_8.

$$\frac{4}{3}Li_2S \rightleftharpoons 2Li^+ + 2e^- + \frac{1}{3}Li_2S_4 \quad (20)$$

$$2Li_2S_4 \rightleftharpoons 2Li^+ + 2e^- + Li_2S_8 \quad (21)$$

Li_2S_8 is further oxidized and eventually precipitates out as S_8 solid.

$$Li_2S_8 \rightleftharpoons 2Li^+ + 2e^- + S_{8(l)} \quad (22)$$

Since the small particles have a larger specific surface area, the dissolution process is faster than the larger particles. A second dissolution reaction is modeled and termed as a redox mediation reaction where the oxidized Li_2S_8 in solution reacts with and promotes the dissolution of Li_2S solids.

$$Li_2S_8 + \frac{4}{3}Li_2S \rightleftharpoons \frac{7}{3}Li_2S_4 \quad (23)$$

This second dissolution mechanism only occurs for the larger Li_2S particles and is independent of cell potential. Similar to the previous two models, this additional precipitation/dissolution phenomenon is coupled with 1D bulk transport in dilute solution with standard mass and charge conservation expressions. They have an additional equation to track Li_2S particle size growth and growth is assumed to be the same across the cathode.

Xiong *et al.* were able to simulate charging curves that mostly match experimental curves from 1C to 2C, shown in Fig. 3. Specifically, they were able to simulate the charging curve with a spike at the beginning that they attribute to higher activation overpotentials due to limited surface area from the large particles. They varied the redox mediation reaction rate to show the effect on voltage and particle size. They also performed simulations with the redox mediation reaction and without. Without this reaction, there are two voltage plateaus seen with the high voltage plateau duration correlated to the volume fraction of large particles. In experimental charging curves with only one voltage plateau observed, they conclude that the charging process differs from the discharge process, where two plateaus are commonly observed, as the large particles dissolve through a redox mediation reaction instead of oxidation.

Danner *et al.*[31] explored fully reversible nucleation and growth through both charging and discharging while keeping track of the particle size distribution of S_8 and Li_2S. They used a two-step classical theory of nucleation and growth to model precipitation/dissolution with the diffusion-limited nucleation rate based on free energy of formation. The nucleation rate is also dependent on the number of nucleation sites, affinity of nucleation to different material surfaces, and specific surface area. The growth step is radial and described as a two-step diffusion to and reaction on the particle surface. Again, the nucleation and growth mechanisms are coupled to 1D bulk mass and charge transport governing expressions through species concentrations and active surface area. This model also includes electrochemical double layer charging at the solid–electrolyte interface and uses an empirical correlation relating electrolyte viscosity to total sulfur concentration. It is worth noting that Danner *et al.* made a good attempt at explaining where each set of parameters comes from.

The simulations from Danner *et al.*'s model for discharge curves and particle size distributions only match Yu *et al.*'s experimental cycling and *operando* XRD data[41] in a qualitative manner (at C/5 and C/10). Surface energy was found to be the most important parameter in a sensitivity analysis with respect to cell capacity. Ability to model the surface energy through atomistic simulations, and to model the impact of changing this surface energy parameter in the above continuum model, can help in selection of electrolyte additives which can modify surface energy. Danner *et al.* also carried out a PITT simulation and found that almost all the Li_2S particles nucleate and form in a short time period after the maximum supersaturation is reached. This time period occurs during a long constant voltage period slightly above 2.1 V, and similar voltage/current behavior has been observed in the experimental literature.[42] PITT experiments, and also simulations, can be useful to look at the minimum overpotential for nucleation initiation that might vary with surface or E/S ratio.

Danner *et al.* then used the same parameters fit from the discharge curves to simulate charge curves, which do not match experimental voltage data well, thus highlighting a parameter or mechanism discrepancy. However, the final particle distribution size of S_8 match well with *operando* XRD,[41] and most Li_2S dissolves before S_8 precipitates. The simulated charging curves show two distinct plateaus at all C-rates with the first voltage plateau being most sensitive to K_{sp,Li_2S}. The authors also simulated a shallow cycling experiment – discharge to 2.2 V and charge using varied C-rates – and found that the small S_8 nucleation feature seen in the upper plateau disappears with increased C-rate due to high overpotentials. Also, at increased C-rates, there is less time to grow and so the S_8 particles are smaller, which agrees with the XRD literature.

All the above models are able to show a decrease in specific capacity with increased rate and attribute ability to predict rate-dependent capacity to the addition of more descriptive nucleation and growth mechanisms. Ren *et al.* and Xiong *et al.*, both papers from the Zhao group, are able to fit their models to experimental data well as opposed to in a qualitative manner. They also model dissolution/precipitation of Li_2S as an electrochemical step while Andrei *et al.* and Danner *et al.* use chemical reactions. A common idea proposed that could utilize these precipitation models to maximize capacity is to seed the carbon electrode surface with preferential adsorption sites or nucleation seeds. This can be done by adding doped sites with high affinity towards Li_2S[31] or catalyst particles.[39] Modeling can be used to optimize the number of initial nucleation sites by striking a balance between size and number of nuclei to promote uniform growth, maximize specific surface area, and prevent large surface oversaturation. Clearly, we still lack a unified model that is able to explain charge and discharge with a relevant set of parameters. The knowledge gap can be alleviated through insights from molecular simulations on kinetic rate parameters and nucleation phenomena. Out of all the charging models in the literature, Xiong *et al.*'s proposed model does the best job of capturing experimental charge features.

An alternative to the nucleation and radial growth theory is modeling precipitation phenomena as 2D *vs.* 3D growth. This can be done through mesoscale modeling as the morphology of the precipitate affects pore space evolution in the cathode. An example of this is Mistry and Mukherjee's work[43] which assumes that there are different energetic interactions between the carbon substrate and the Li_2S precipitate. Because of this, precipitate morphology can range from depositing at the carbon–pore interface, leading to more film-like structures (2D) or precipitates self-depositing at the precipitate–pore interface, leading to more finger-like structures (3D). Mistry and Mukherjee vary this morphology factor in a coarse-grain mesoscale model based on deposition energy involving surface affinity. They found that low-order morphologies lead to surface passivation, and high-order morphologies lead to pore blockage. These two events lead to cathode starvation – no active reaction area – and no further reaction can happen, causing the cell voltage to drop. Importantly, they showed the effect of microstructure evolution on electrochemical performance by relating mesoscale level variables (morphology factor, porosity, precipitation amount) as effective microstructural properties (tortuosity, conductivity, active area) that are used in a continuum-level electrochemical model. This meant that they could show the effect of morphology or porosity on cell operating condition trends such as capacity dependence on C-rate.

This is a good example of multiscale modeling where modeled mesoscale interfacial phenomena is coupled with macroscopic cell-level performance. Note that pretty much all the existing meso/micro-scale models have not reported on mesh convergence/simulation efficiency and error. For a recent paper on the importance of mesh convergence, in particular in the presence of corner singularities, see ref. 44.

We can borrow insights from models at a smaller atomistic scale too. First-principles DFT calculations can show the strength of interaction between Li_2S in solution and an adsorbed solid Li_2S site.[45] Liu and Mukherjee created a coarse-grained lattice-based mesoscale model and used KMC to simulate Li_2S adsorption, desorption, and diffusion on the surface. Since the nature of growth is related to fundamental interactions (pore/solvent structure *etc.*) that manifest as surface energetics, engineering of carbon structure and electrolyte to make it unfavorable for 2D film formation is an area of research with plenty of opportunity to be driven by a combination of atomistic, mesoscale, and continuum models.

Cathode structure

The development and optimization of structured cathodes[46,47] has gained a lot of attention as a strategy to mitigate low sulfur utilization. Because both S_8 and Li_2S solids are insulating, strategies to overcome poor electronic conduction are important in achieving high sulfur utilization. Cathode structure is also important for polysulfide entrapment to mitigate shuttling and to combat volume expansion during lithiation. However, most of the continuum modeling literature assume a macroscale composite carbon/sulfur cathode with effective properties, captured by the electronic conductivity, carbon fraction, and active surface area. More sophisticated microscale models are needed to understand the complex behavior and structure of the cathode. A study by Danner *et al.*[11] explored the implications of a nanostructured cathode with meso- and micro-porous carbon particles. Their work employed a simplified reaction scheme with a 1 + 1D model, where all the polysulfides remain trapped within the particles; their modeled cathode is similar to the porous electrode pseudo two-dimensional (P2D) model, where transport through the cathode and into the particle is considered. Comparing with experimental data, the model captured trends but missed the plateau transition and end of discharge regions, most likely due to the simplified 2-step reaction mechanism. Their work explored the effect of sulfur loading and salt concentration on the voltage and the simulated pore volume fraction. With lithium-ion as the sole charge carrier, the transport overpotential is significant to overcome the concentration gradient.

Work by Thangavel[48] describes a structured cathode with mesoporous carbon particles. The model includes transport on two different scales, within inter-particular pores (between carbon particles) and filling the mesopores of the carbon particle. The model also captures Li_2S film passivation on the surface of the particles and within the mesopores. The work explored the sensitivity of microstructural properties on the discharge capacity. The predictions were able to reproduce rate capability seen experimentally.[49–51] When considering particle and mesopore sizes, the discharge capacities of larger particles were lower than small particles due to decreased surface area. The large particles showed faster Li_2S film thickness growth, which led to earlier choking of the mesopores within the carbon particle and leaving unutilized sulfur. The Li_2S film passivated the cathode, resulting in lower voltage. Meanwhile, the smaller particles had a higher discharge capacity overall; the clogging of the inter-particular pores signaled the end of discharge because the Li_2S film did not reach the threshold thickness for choking the mesopores. The effect of C/S ratio was also explored by varying the sulfur loading; the highest sulfur loadings also exhibited the lowest capacities. The results from this work suggest that the microstructural properties can be tuned to delay the negative effects of Li_2S(s) precipitation; the highest surface area for particles is recommended to alleviate clogging and film growth that leads to passivation of the cathode and poor sulfur utilization. Microscale models more accurately represent the competing phenomena of pore clogging and surface passivation and can guide design of the cathode. Furthermore, continuum models may need guidance from statistical-based models, such as KMC, or molecular dynamics to further understand evolution of the cathode dynamics and derive experimentally relevant parameters. The structure and material of the cathode is also highly engineered to suppress shuttle, and with guidance from DFT, adsorption and diffusion of polysulfides can be found,[52] and these values can be expressed as continuum level transport properties.

Shuttling, degradation, and lithium anode dynamics

Continuum modeling papers focused on lithium–sulfur have traditionally modeled the anode as a flux boundary condition (lithium foil that supplies unlimited lithium ions), as a protected anode domain with Butler–Volmer kinetics describing the lithium redox reaction (although the anode overpotential is commonly taken to be negligible due to evidence that the cathode overpotential is dominant[13]), or as an active participant in the reduction of polysulfides that have shuttled over and in passivation reactions involving polysulfides at the anode surface. A few papers have modeled the effects of shuttle on the anode surface by approximating passivation with decreasing electrochemical active surface area, which changes the reactivity of the surface and affects the overpotential of lithium oxidation; this represents a first step towards understanding the impact of the lithium metal anode and consequent degradation and side reactions on cell operation. For high specific capacity batteries, we anticipate that future models will include both electrodes with experimentally-derived mechanisms, using a suitable electrolyte, to best represent a state-of-art cell. In all the models reviewed in this paper, SEI and dendrite formation on the lithium metal anode are not considered although they are important phenomena that remain hurdles for commercialization of lithium metal batteries. Models with detailed dendrite growth modes to describe lithium metal

electrodeposition and stripping[53–55] can be coupled with 1D electrochemical models[56,57] to describe the lithium metal system. Understanding the behavior of the lithium metal anode in tandem with the complex polysulfide speciation behavior will give insights into cell design and operation to overcome current cycle life limitations. First-principles calculations and atomistic simulations can also shed light on electrolyte decomposition[58] and film formation[59] on the anode; the calculated molecular-level reaction and surface energies can be incorporated as side reaction rate constants and passivation rates in continuum models.

The main degradation mechanism for lithium–sulfur batteries is the shuttle phenomena. During charge, lithium ions that are liberated from the cathode travel to the anode to be reduced to lithium metal to store the incoming charge. Since the polysulfides are also soluble in the electrolyte, they diffuse to the anode and are reduced as well, consuming the electrons meant to be stored there. The reduced polysulfides then travel back to the cathode and can be oxidized, only to repeat the process. Additionally, lower-order polysulfides may react with lithium at the anode to produce Li_2S(s) that can further contribute to passivation of the anode and cell resistance.[33] Understanding the shuttle phenomena is key to development and operation of long-life high energy density lithium–sulfur batteries. The modeling literature has approached the study of shuttle with both 0D and 1D models using macro- and micro-scale mechanisms.

The first 0D model by Mikhaylik and Akridge[10] included the shuttle degradation as consumption of the higher-order polysulfides at the anode during the higher plateau. The rate of shuttling is proportional to the concentration of higher-order polysulfides multiplied by the shuttle reaction rate (second term of eqn (24)) and is included in a mass conservation differential equation:

$$\frac{d[S_H]}{dt} = \frac{I}{q_H} - k_s[S_H] \tag{24}$$

where $[S_H]$ is concentration of higher-order polysulfides normalized to specific volume or surface, I is the normalized charge/discharge current, q_H is the sulfur specific capacity for the higher voltage plateau, and k_s is the shuttle rate constant. Shuttling only occurs during charging and is assumed to start during the second cycle. The model also included self-heating from the shuttle current and an Arrhenius expression to describe the temperature dependence of the shuttle rate. Their model also focused on overcharge protection due to infinite charging. This happens when the shuttle current is equal to or greater than the applied current, and the voltage curve levels off into a plateau *ad infinitum* with no increase in the stored charge.

Another 0D model with the shuttle mechanism is the study by Marinescu *et al.*[60] In their work, a fraction of the shuttled polysulfides becomes permanently inactive, described by a dimensionless loss rate, f_s. The rate of shuttle or loss sulfur, S_l, is proportional to the mass of dissolved sulfur, S_8^0, the shuttle rate constant, k_s, and the sulfur that has already been shuttled, S_s, which means that the shuttle rate increases with aging.

$$\frac{dS_l}{dt} = \frac{f_s}{m_s} S_s k_s S_8^0 \tag{25}$$

where m_s is the mass of active sulfur per cell. The authors relate the increased rate of shuttle to increased surface area available for precipitation as more solids precipitate on the anode although in a lumped model the sulfur loss is area nonspecific. The model is used to explore experimentally seen voltage drift with cycling, and the authors attributed it to SOC drift. Therefore, traditional SOC estimation techniques like coulomb counting or voltage reading are not adequate for cycling of LiS batteries. The model also classified capacity loss as either reversible or irreversible, depending on the conditions. Predictions from the model indicated that reversible capacity loss is due to the bottleneck of slow dissolution of solids from high charging rates while irreversible capacity is due to shuttle at low charging rates.

The description of the shuttle phenomena with a 0D model inherently ignores the transport of the polysulfides from the cathode to the anode. Several 1D models have incorporated the shuttle as a microscale mechanism to understand the role that transport plays in degradation. Hofmann *et al.*[61] explored the polysulfide shuttle mechanism with the simplified 2-step reduction scheme. Their mechanism included the reduction of S_8 to S_4^{2-} and precipitation of Li_2S at the anode; furthermore, the Li_2S at the anode is classified as either active or passivating the surface. The passivating Li_2S decreases the anode reactive surface through a heuristic expression

$$f(\varepsilon_S) = \left(\frac{\varepsilon_{pore} - \varepsilon_{Li_2S}}{\varepsilon_{pore}}\right)^{3.5} \tag{26}$$

where $f(\varepsilon_S)$ approximates the active surface on the anode, ε_{pore} is the volume fraction of usable anode, and ε_{Li_2S} is the volume fraction of passivating Li_2S on the anode surface. This heuristic approximates the degradation of the anode surface through loss of electrochemical active area. As the cell degrades, resulting in both loss of active material and less reactive surface area on the anode, the anode overpotential increases, decreasing the voltage plateaus. The model predicts higher capacity loss per cycle initially, which levels off; this is in agreement with experimental studies that show high capacity loss during the initial cycles.[62]

Another study by Yoo *et al.*[35] uses the 5-step reduction scheme with the shuttle mechanism at the anode. During charge, the polysulfides are able to travel to the anode, where they are reduced at a rate proportional to their concentration and their individual shuttle constant; this represents lost charge due to shuttle.

$$\left.\frac{\partial C_i}{\partial t}\right|_{x=L_1+L_2} = -k_{ps,i} C_i + k_{ps,i-1} C_{i-1} \tag{27}$$

where k_{ps} is the shuttle rate constant. The first term is the sink while the second term is the source from a higher-order sulfur species denoted with $i - 1$. The model does not include precipitation of solids on the anode surface. This work explored cycling performance of cells with various diffusivities and reduction rates; predictably, the degradation worsened for high

diffusivities of polysulfides and increased reduction rates. Kamyab *et al.*[63] followed a similar approach to including shuttle on the anode, where the rate of precipitation is proportional to the shuttle rate and concentration.

Mistry and Mukherjee[9] extended their previous work using concentrated solution theory to study the effects of speciation and lean electrolyte conditions on polysulfide shuttle and degradation. The shuttle is modeled as an interfacial flux due to the redox reaction at the anode/separator interface, shown in Table 1 (when modeling without shuttle, flux at the interface is zero for all species except lithium). The capacity loss is characterized as either reversible or irreversible, due to reduction of higher-order polysulfides at the anode or precipitation of Li_2S on the anode surface, respectively. With increasing C-rate, the overall capacity loss due to shuttle decreases due to decreased operation time. However, the limitations from the cathode and electrolyte have the largest contribution at high C-rates, indicating an optimum intermediate rate to balance degradation phenomena. This is in contrast to the macroscale/0D modeling of shuttle, where capacity loss increases with rate. Taking a closer look at electrode conditions, E/S ratio and porosity show a nonlinear relationship with limiting phenomena. At lower E/S ratios and porosity, the transport limitations dominate while increasing these parameters leads to capacity loss from polysulfide shuttle. Incorporating a detailed model for lithium metal morphology will allow a closer look at the relationship between shuttle, speciation, and high energy cell conditions.

The study by Danner *et al.*[11] explored degradation with nanostructured cathodes where all of the polysulfides except for S^{2-} are assumed to be trapped within the carbon particles. After S^{2-} diffuses out of the particle, the model assumes that it is now electrochemically inactive representing the maximum amount of irreversible loss of sulfur; realistically, the diffused S^{2-} could still participate in reactions as long as it is within the cathode matrix. The capacity loss is linear initially and then increases steeply with more cycles. This work also explored the effect of Li_2S solubility product and salt concentration on the cycling capacity loss. With higher K_{sp} for Li_2S, more of the S^{2-} is able to leave the particle resulting in increased loss. The cycling study shows that increasing the salt concentration increases capacity retention; however, high salt concentrations will have a negative effect on both ionic conductivity and the energy density of a cell. This work highlights the importance of modeling to optimize multiple variables simultaneously for practical high energy cells.

Polysulfide shuttle can also occur in the absence of current and can lead to self-discharge. This is due to the lithium anode being strongly reducing. To understand the self-discharge behavior due to shuttling, Al-Mahmoud *et al.*[64] fabricated LiS cells with varying numbers of separators between the electrodes, and measured the voltage signal measured from a fully charged state. The 1D model considers transport through the separator and redox reactions at the electrodes as boundary conditions; the only species in the model are S_8 and S_8^{2-} that continuously oxidize or reduce at the electrodes. The net current is zero, and the current that oxidizes S_8^{2-} is equal to the change in potential multiplied by the capacitance of the carbon. Mahmoud *et al.* found that including the capacitive behavior of the carbon within the sulfur cathode was necessary to reproduce the open circuit potential of a battery with 5 separators. Without including the capacitance, the voltage sharply drops, leveling off within 30 minutes, while the model with capacitance predicts a gentler slope to the final voltage at around 2 hours, matching the experimental curve. Their simple model can predict the evolution of the open circuit potential of batteries well with 2 to 5 separators. The model was also able to capture the difference between the self-discharge behavior of a cell with no initial dissolved sulfur and a cell with saturated electrolyte by altering the initial conditions of sulfur in the electrolyte.

Another approach of measuring and modeling the shuttle current during self-discharge was demonstrated by Moy *et al.*[65] They measured the shuttle current by holding the electrode potential constant and waiting till the current reaches a steady state value. The steady state current is equal to the diffusional flux of polysulfides between the electrodes. They found that the shuttle current decreases to zero with depth of discharge since insoluble products are present at the end of discharge. They also found that with the addition of $LiNO_3$, the shuttle current is reduced to almost zero due to $LiNO_3$ forming a passivation layer on the anode. With a simple model based on algebraic equations of flux balances, and the assumption that the anode is strongly reducing such that all higher order polysulfides are reduced to S_4^{2-} at the anode, Moy *et al.* were able to model the shuttle current as a function of SOC that match experimental values well. They also assumed linear concentration gradients from diffusive fluxes and that the conversion of S_4^{2-} to Li_2S_2 and Li_2S solids at the anode is 100–3000 times slower than the interconversion of polysulfides and hence do not model this process in their calculations of shuttle current. However, this phenomenon is observed in their experiments in the form of the slow decay of shuttle current at long timescales. Moy *et al.* used an average value of this decay rate over a discharge cycle and calculated irreversible capacity fade as a function of cycle life. Being able to quantify the shuttling rate with SOC and shuttle decay is important to help predict the effectiveness of modifications without excessive cycling.

Research by Wen *et al.*[66] modeled self-discharge in a 1D LiS sandwich cell to explore reversible *versus* irreversible capacity loss. The self-discharge behavior of coin cells at different cycles was explored, and the cells underwent *ex situ* X-ray diffraction experiments to analyze precipitation. The relationship among self-discharge, polysulfide shuttle, and the resting voltage was proven to be important and rate-dependent. Self-discharge was more rapid at higher voltages due to higher-order polysulfide reduction at the anode; the capacity loss was highest at high SOCs. Resting during the lower voltage plateau leads to formation of precipitate and minimal capacity loss. The authors recommend resting at 2.10 V to minimize capacity loss, and the model results indicate that the focus should be on anode protection to mitigate degradation.

Multiple phenomena, such as intermediate polysulfide transport and lithium metal passivation, play an important and

complex role in both calendar and cycle life, and continuum modeling has furthered our understanding of degradation through incorporating these mechanisms. Moving forward, models should include more detailed dynamics of the lithium metal surface evolution for a full cell view of these issues.

Transport properties, limitations, and solution phase dynamics at low E/S ratios for a cell

It is important for a model to capture transport limitations in a cell to mimic conditions such as a battery with low E/S ratio undergoing fast charging. In the 1D literature, the resistance within the electrolyte is not adequately captured.[34] Experimentally, ohmic resistance as a function of state-of-charge (SOC) can be measured using EIS (the high frequency real-value limit). In the case where electronic conductivity is high, electrolyte resistance can be assumed to be the bulk of ohmic resistance. To adequately capture electrolyte effects, both micro and macroscale liquid phase dynamics have been incorporated.

Zhang *et al.*[34] calculated the variation of the electrolyte resistance with SOC using the Kumaresan model and found that this variation does not match experimentally measured electrolyte resistance. To accurately represent the electrolyte transport in a macroscale manner, Zhang *et al.* expressed electrolyte conductivity as a linear function of Li^+ concentration, which represents the sum of anion concentrations since measurement of transport properties of each individual polysulfide anion is challenging. With this expression of ionic conductivity,

$$\kappa = \varepsilon^{1.5}(\kappa_0 - b|C_{Li^+} - C_{Li^+,0}|) \quad (28)$$

where ε is porosity, κ_0 and b are fitted parameters, and C_{Li^+} is the concentration of lithium-ion with $C_{Li^+,0}$ being the initial concentration, they introduced two new parameters and were able to reproduce both the trend and magnitude of the electrolyte resistance during discharge from experimental data. This result is shown in Fig. 4. We note that they used a 0D lumped model without mass transport (reactions modeled off Kumaresan *et al.*) and incorporated the electrolyte resistance as an ohmic potential drop contribution in the overall cell voltage. Zhang *et al.* found that the voltage dip during the transition between the two plateaus occurs not only due to supersaturation of S^{2-} but also due to a peak in electrolyte resistance, consistent with modeling results from the concentrated solution model by Mistry *et al.* (reviewed later in this section).[67] Other papers have also used expressions of ionic conductivity as a function of lithium ion concentration and these are empirical expressions found using fits to experimental conductivity data.[38,39] These papers represent a macroscale view of modeling effective transport properties.

For a high energy density cell, the E/S mass ratio should be less than 5 μL mg^{-1},[5] hence a lean and concentrated electrolyte would mean solubility and transport limits sulfur utilization. Also in line with macroscale modeling, Zhang *et al.*[14] reduced the diffusion coefficients of all species by two orders of magnitudes to demonstrate a transport-limited cell. They use a 1D Kumaresan-type model with the only precipitate being Li_2S. They are able to match experimental discharge curves qualitatively, with the ability to capture the reduction of the low plateau capacity at higher currents which has not been shown previously. However, they were unable to capture curvature of the first plateau and some features at higher rates. To test their theory of the cell being transport-limited, they carried out an experiment and corresponding simulation where the cell is discharged, relaxed, and allowed to be discharged further. Since some capacity is recovered after relaxation, Zhang *et al.* concluded that for a high energy density LiS cell, the discharge capacity reduction due to higher current can be attributed to transport limitations, and less so due to surface passivation or pore blockage from precipitates. If transport is indeed a limiting factor for LiS cells, models might need to move away from the macroscale dilute solution theory towards a concentrated solution theory to better capture diffusive effects.

For a microscale approach, using recent nucleation and growth models that are able to predict reduction in capacity of the lower plateau with increasing rate, Andrei *et al.*[39] repeated

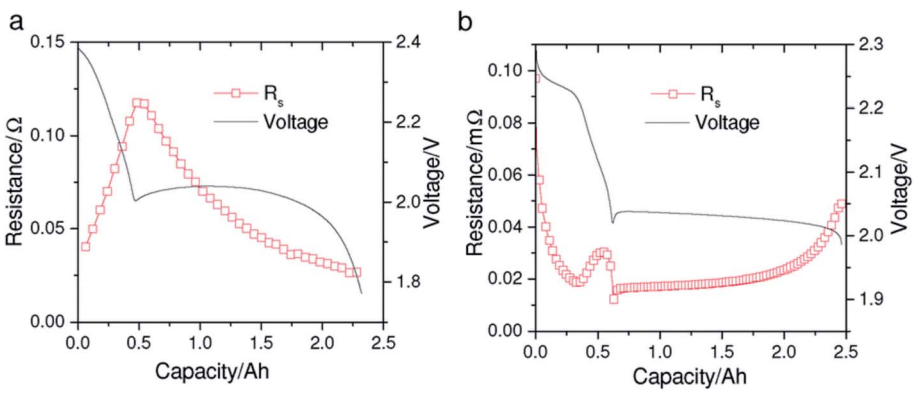

Fig. 4 Discrepancy between experimental and modeled electrolyte resistance as a function of depth of discharge. (a) Electrolyte resistance of a commercial LiS pouch cell measured using EIS. (b) Simulated electrolyte resistance from the ref. 8 model. Reproduced from ref. 34 with permission from the PCCP Owner Societies.

an experiment by another Zhang *et al.*[36] paper. Andrei *et al.* used a 0.2C–1C–0.2C variable discharge rate and compared the specific capacity of certain portions to a standard 1C discharge. Their results did not match Zhang *et al.*'s conclusion that rate-dependent discharge capacity is due to slow transport (here, Andrei *et al.* are unable to recover all capacity at a slower rate), but rather found that different dynamics of nuclei growth occurs at different C-rates. There is a disagreement between the nucleation papers[38,39] and the Zhang *et al.*[14,36] papers about whether capacity reduction at high discharge rates is due to rate-dependent surface coverage or rate-dependent transport limitations. Furthermore, Zhang *et al.* used EIS to show that charge transfer resistance, commonly associated with surface coverage, is SOC-dependent and rate-independent. The discrepancy in experimental results is likely due to Andrei *et al.* using coin cells with low loading while Zhang *et al.* used OXIS pouch cells with presumably low E/S ratio. There needs to be a clear understanding that a single model will not be able to capture different limiting phenomena due to differently engineered cells. Comparing their simulations to an experimental cell with lean electrolyte, Zhang *et al.*[36] used a simple 0D model with a modified transport-limited Butler–Volmer kinetics expression (includes limiting current):

$$\frac{I_j}{a_v V i_j} = \left(1 - \frac{I_j}{I^{\lim}}\right)\exp\left(\frac{-F\eta_j}{2RT}\right) - \left(1 + \frac{I_j}{I^{\lim}}\right)\exp\left(\frac{F\eta_j}{2RT}\right) \quad (29)$$

where I_j is the current of reaction j, i_j is the exchange current density, a_v is the specific surface area of the cathode, V is cell volume, $I^{\lim}$ is the limiting current due to mass transfer. Not only were they able to match their variable discharge rate experiment very well, but they are also the first model to demonstrate the kink at the start of charging. Review of these two papers demonstrate the complicated nature of lithium–sulfur systems and the existence of competing phenomena. We want to highlight that the cell conditions dictate the limitations and ultimately there should be a model that can accurately predict both precipitation phenomena and transport limitations in line with experimental work.

An improvement to prevent shuttling is to use gel polymer or gelled liquid electrolytes to trap polysulfides by limiting their transport and solubility. Gel electrolytes are also less flammable and help suppress dendrites at the lithium anode. Shebert *et al.*[68] effectively combined experiment and simulation to explore mass transport limitations introduced by gel electrolytes. Through experimental work, they showed that the specific capacity of a liquid electrolyte system is still better than the gel electrolyte systems, though the cycling performances of the gel electrolyte systems are better. They also showed that for an LiS cell with gel electrolyte, the first discharge voltage plateau is extended while the second plateau is shortened, relative to a conventional electrolyte. The former effect suggests that the gel electrolyte system promotes entrapment of polysulfides and improved sulfur utilization. This latter effect implies slow conversion of soluble to insoluble polysulfides and could be due to slow transport of intermediate polysulfides or passivation of reaction sites. To investigate this, Shebert *et al.* conducted an experiment where they discharged a cell to 1.8 V, let it rest for an hour, and discharged it further. They showed ability to recover more capacity in the second discharge, which indicates that this effect could not be due to all polysulfides being reduced or all sites being passivated, but rather due to mass transport limitations. The gel electrolyte system had greater capacity recovery than the liquid electrolyte system. Shebert *et al.* also varied the pause time and measured capacity recovery as a function of C-rate. Then, they were able to match their experimental results qualitatively using a continuum model with a fast and slow diffusion rate of S_4^{2-} (slower diffusion represents the gel system). Similar to Zhang *et al.*,[36] they used a mass-transport limited Butler–Volmer expression to model kinetics of the electrochemical reactions; however, this is a 1D instead of a 0D model. In this model, the limiting reaction rate has two extra fitting parameters with the assumption that the maximum mass transport rate to reaction sites decrease as solid deposits clog the pores in the cathode and the bulk concentrations of reactants decrease. For the discharge–pause–discharge experiment, during the pause, S_4^{2-} has time to diffuse back to the cathode to get additional capacity. Mass transport limitations are only seen at the end of discharge when there is low concentration of S_4^{2-} and a lot of surface passivation from Li_2S deposits. Since the discharge capacity of LiS cells with gel electrolytes is still smaller compared to conventional electrolytes, this investigation shows that the capacity can be improved by limiting the polysulfide flux out of the cathode or speeding their return to the cathode.

Transport properties can also be modeled in a microscale manner to consider the effects of complex solvent interactions. Mistry *et al.*[67] developed a 1D model based on concentrated solution theory that describes the complex transport behavior during discharge. Concentrated solution theory, derived from nonequilibrium thermodynamics, captures interactions among the polysulfides by accounting for the self- and inter-species transport at high concentrations. The fluxes are defined by the following:

$$N_i = -D_{ii}\nabla C_i - \sum_{j\neq i} D_{ij}\nabla C_j + t_i\frac{I}{z_i F} + C_i V_0 \quad (30)$$

where N_i is the flux for species i. The first term is the self-gradient flux where D_{ii} is the diffusion and C_i is the concentration of species i. The second term is the contribution of dissimilar species to the diffusion where D_{ij} is the cross-diffusivity and C_j is the concentration of species j. The third term describes the migrational contribution to flux, where t_i is the transference number and z_i is the charge number. The final term is due to advection of the bulk flow of the species due to solvent motion where V_0 is the velocity of the solvent. Within this model, the limitations due to surface passivation from insulating precipitates, pore blockage, and electrolyte resistances are calculated and compared. The work uses a microstructurally resolved model to describe the changing morphology during discharge. They attributed part of the voltage recovery before the second plateau to ionic conduction of medium chain polysulfides, in agreement with Zhang *et al.*[34] The dominant species that contribute the most to high concentrations and consequent transport limitations are Li^+

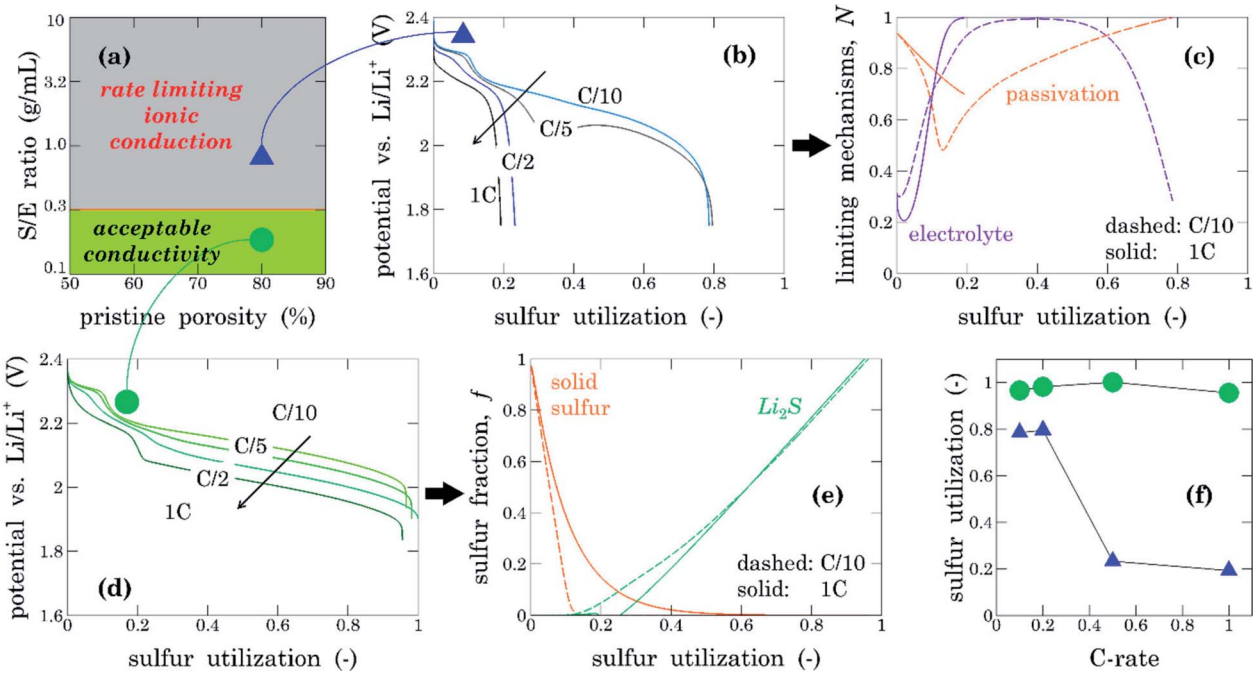

Fig. 5 Electrolyte transport regimes, (a) porosity *versus* S/E (sulfur to electrolyte) ratio with green showing acceptable conductivity and higher values in the rate limiting ionic conduction, (b) potential curves within the rate limiting regime, (c) plot showing the limiting mechanism with sulfur utilization, (d) potential curves with acceptable conductivity, (e) solid species with sulfur utilization, (f) shows the sulfur utilization with C-rate for both regimes. Reprinted with permission from ref. 67. Copyright 2018 American Chemical Society.

ions due to accumulation until Li_2S precipitation, and medium-chain polysulfides (S_4^{2-}) due to solubility and higher production rate compared to the higher-order polysulfides. The model is able to capture competing dynamics, like the rate dependence of passivation, pore blockage, and ionic conduction. Their work classifies E/S ratio in two regimes, rate-limiting and acceptable, shown in Fig. 5. When considering the rate-limiting ionic conduction with low E/S ratios (or high S/E ratios), the sulfur utilization is highly C-rate dependent (Fig. 5f). At low rates, the ionic conductivity increases with an increased rate due to overlap in the speciation; consequently, there is a lower concentration of medium-chain polysulfides, resulting in less transport resistances. This is balanced with increased potential drop due to transport limitations of higher rates. For the increase from C/10 to C/5, shown in Fig. 5b, there is an increase in sulfur utilization. However, at higher rates, the increased ionic conductivity is not enough to overcome the resistance due to transport at higher rates (Fig. 5c). For acceptable conductivity behavior (Fig. 5d and e), the sulfur utilization is fairly constant with C-rate, and there is a decrease in the voltage for increasing rate. Within a practical high energy density cell, the conditions are expected to cause high concentrations and viscous electrolyte conditions, highlighting the importance of studying electrolyte transport limitations through this lens.

Considerations for scale-up and high energy density cells

Testing and development of new battery materials first occur on the coin cell scale. Many times, the results from coin cell experiments fail to scale up for larger-format cells.[69] Coin cells often have excess electrolyte resulting in flooded cell conditions. In a flooded cell, the excess electrolyte masks limitations and is not practical for high energy cells. In particular, the negative effects of electrolyte consumption are delayed, and issues surrounding cell wetting or transport limitations due to viscous solutions and high concentrations of polysulfides are masked by the excess electrolyte. Flooded cells mean higher cost and lower energy density. There has been a concerted effort to set standards for cell conditions to test high energy format cell conditions.[70] The E/S ratio is an important metric that describes the volume of electrolyte to the mass of sulfur. It has been calculated that high energy cells should have an E/S ratio of less than 5 μL mg^{-1}.[5]

Modeling tools can help explore the effect of E/S ratio. Previous work by our group[26] explained that the original model formulation from Kumaresan[8] is not able to replicate appropriate E/S ratios for high energy density cells. For the 1D lithium–sulfur model, the sulfur/carbon/porosity are all constrained, and the E/S ratio is simply a calculation based on the ratio of the sulfur volume fraction to porosity within the cell. The porosity is constrained by sulfur mass conservation while the electrolyte volume is not explicitly conserved. However, within a real cell, electrolyte amounts are not completely constrained by the porosity, sulfur loading, and filler fractions since overfilling or underfilling can occur. The E/S ratio for the 1D model work greatly underestimates the E/S ratio. Another aspect that is not captured currently within models is the wetting of the cathode. The modeling literature assumes perfect wetting and effective cathode properties. However, for E/S ratios for a practical high energy cell, the problem of cathode wetting is very

relevant as high carbon content reduces wettability due to solvophobicity of carbon.[5] Perhaps development of microscale models that study the interactions among sulfur, carbon infrastructure, and electrolyte would be insightful to optimizing E/S ratio and other important metrics for high energy cells. Modeling groups will facilitate better communication with experimentalists by reporting and calculating important metrics like E/S and C/S ratios in their work. Closer collaboration with molecular simulation groups is recommended to help model physical interactions and provide relevant parameters.

A series of papers by the Eroglu group[13,71–74] have investigated both E/S and C/S ratios in their macroscale modeling work. Their work coupled cell-level predictions of voltage, overpotentials, and area-specific-impedance with systems-level predictions of energy densities from the publicly available software called Battery Performance and Cost (BatPaC). The 1D model is used to predict the effect of E/S ratio on voltage and capacity trends. Coupling the results with the calculations from BatPaC, the cell-level specific energy and energy densities can be calculated for various sulfur loadings and maximum thicknesses. This work extends optimizing for capacity to systems-level parameters that are relevant for commercialization. For example, increasing electrolyte amount improves both voltage and capacity, but the excess material comes at a specific energy penalty. With the electrochemical predictions feeding into the cell-level model, the balance between improved performance and energy density can be understood. The model predicts the best performance with an E/S ratio of 20 μL mg^{-1}, but E/S = 13 μL mg^{-1} provides an optimum for specific energy and energy density. This result is surprising as the E/S ratio is higher than what is typically considered desirable for state-of-art cells. For example, with high E/S ratios of over 11 mL g^{-1}, the pouch cell specific energy will be below 140 W h kg^{-1}, less than advanced Li-ion batteries.[69,75] This highlights the need to push for consistent and relevant metrics to relate models to high performing LiS cells.

Electroanalytical methods for whole cells

Electroanalytical techniques can be useful to provide information on mechanisms and physical processes beyond what we can learn from standard charge/discharge voltage curves. For example, we looked at work in the Cathode reaction scheme section where CV was modeled as a means to propose reaction pathways.[20,22] There might be other ways to disaggregate physical processes from each other. For example GITT is commonly used to find diffusion parameters in lithium-ion systems but has only been used experimentally in lithium–sulfur systems to look at internal resistance[76] and thermodynamic equilibrium.[33,77,78] There has been work done to apply diffusive concepts from GITT theory to a lithium–sulfur cell using a simplified example system[79] but no lithium–sulfur continuum model has been applied to understand thermodynamics separately from transport and kinetic processes. However, PITT has been simulated by Danner & Latz[31] (more detail in Precipitation section) to explore nucleation overpotential.

Another useful electroanalytical measurement is EIS, which can separate processes occurring on different time scales. For lithium–sulfur cells, EIS measurements are commonly fitted to equivalent circuit models and circuit elements that represent physical processes, such as charge transfer resistance, are quantitatively compared. For example, Lee *et al.*[80] compared the magnitude of the charge transfer resistance of a cell with and without a coated separator to suppress shuttling. There have been detailed studies[81–83] using equivalent circuits to fit to EIS measurements at different SOCs, states-of-health (SOHs), and temperatures, but it remains challenging to elucidate the origins of each feature (*e.g.* multiple semi-circles). Physics-based models can help improve diagnostics by attributing specific features to physical processes compared to degenerate equivalent circuit models. Fronczek and Bessler[84] are the only authors that have demonstrated the use of full physics-based continuum models to simulate impedance of LiS cells. They use a similar set of governing equations and reaction schemes to Kumaresan[8] except that the kinetic reactions are written as elementary steps following Arrhenius law instead of Butler–Volmer expressions.

$$\dot{s}_i = v_i\left(k_{\text{fwd}}\prod_j a_j^{v_j'} - k_{\text{rev}}\prod_j a_j^{v_j'}\right) \tag{31}$$

$$k = k_0\exp\left(-\frac{E^{\text{act}}}{RT}\right)\exp\left(-\frac{\alpha z F}{RT}\Delta\phi\right) \tag{32}$$

where $\dot{s}_i$ is the rate of reaction i, v are stoichiometric coefficients, k are forward and reverse rate constants, a_j are activities of species j, E^{act} is activation energy, z is number of electrons transferred, and $\Delta\phi$ is the potential difference between solid and electrolyte. They also included an electrochemical double layer which is important for fast timescales. Fronczek and Bessler simulated the impedance using a voltage step of 1 mV in 0.1 microsecond, and took the fast Fourier transform of the current relaxation over 1000 s. They showed the ability to simulate EIS spectra but with very limited discussion on the results. Their simulated impedance also decreased in magnitude with SOC which does not agree with the experimental literature listed above. This disconnect might be due to the parameters used in their model, the concentration dependent ionic conductivity highlighted by Zhang *et al.*,[34] or other missing mechanisms in the model.

The field can greatly benefit from using a variety of electroanalytical techniques to validate a model to uncover underlying physics that dominate behavior and cell performance. There is also opportunity for the above continuum models to be applied to electroanalytical methods and explore how they are analyzed as functions of state of the cell such as SOCs.

Parameter identifiability and estimation of cells

A natural next step after model development is parameter identification through estimation. If the purpose of a model is to eventually be used in a BMS for control purposes such as

optimal charging, then online state estimation is important for identifying parameters that define the most current state of the battery. Parameter identification is a daunting optimization task for a highly nonlinear system. Some strategies to approach this would be conducting a sensitivity analysis to understand the physical range and impact of varying parameters, careful model reduction to improve computation efficiency (as fitting a model requires running it iteratively),and building frameworks for online optimization.

Ghaznavi and Chen wrote a series of three papers covering sensitivity analysis of the Kumaresan model with respect to different sets of parameters. Their objective was to explore the possible range of physical parameters and mathematical limits of the model. In their first paper,[85] they studied the effect of discharge rate and electronic conductivity on cell performance. They found that at high rates and low conductivity, large amounts of Li_2S precipitate close to the cathode/current collector interface and fill up the porous matrix, thus reducing active surface area. This type of study might be useful when looking at additives or binders to improve conductivity. In their second paper,[29] for the case where intermediate polysulfides precipitate and block pores, they found an upper limit for the optimal sulfur content for greater capacity (only cells with less than 20% sulfur content by cathode volume can be fully discharged). They also varied the precipitation rates for each reaction and found a "critical interval" for each rate constant, where a small variation in rate constant results in a large change in voltage response and capacity. These findings are only for this set of parameters and for the case where we are considering intermediate polysulfides precipitating, which is not typically considered since they are highly soluble. Although in the context of low E/S ratios, it is possible the polysulfide species may precipitate out due to high concentrations. A thorough study with physical parameters (such as solubility) that are relevant for a state-of-art cell, and precipitation mechanisms that can be cross-referenced with experimentally observed species might be more useful to build representative models.

In their third paper, Ghaznavi and Chen[30] first looked at the effect of exchange current densities. By changing the exchange current densities relative to each other, they can determine the dominant reaction and observe shifts in the voltage plateau. This might be useful for elucidating the rate-limiting steps to engineer specific improvements for kinetics. The diffusion coefficients were also varied where a decrease in an order of magnitude showed no effect. They explored optimal cathode thickness and also the need to increase the solubility product by a factor of 10^8 for the model to charge. This set of papers was useful to understand the impact of each physical parameter and demonstrated the ability of models to predict and optimize cell performance in relation to an engineered change. However, this theoretical study based on assumed parameters needs to be taken a step further to align with experimentally observed and measured parameters, trends, and speciation.

Work by our group[86] focused on reducing the computational demand of the standard 1D model by considering each region as a tank connected in series. The Tank-in-Series model has connected mass flow between the regions through continuity of flux; a new fitting parameter describes the fraction of each region where gradients are assumed to be, usually $\frac{1}{2}$ or $\frac{1}{3}$. The reduced model is able to reproduce the trends shown in the 1D model under even transport-limited conditions. A parameter study of rates (up to 1C), diffusion coefficients (as low as to 1×10^{-12} m^2 s^{-1}), and cathode thicknesses explored the suitability of the model predictions under various conditions. A map of the errors was calculated and shown to be under 25 mV for all conditions with most errors falling below 15 mV. The Tank model was calculated to run in under 1 second, representing a speed increase of over 150× compared to the 1D model; the model also implements a logarithmic scaling of the differential variables, resulting in a more robust model that can simulate to lower voltages at the end of discharge where the 1D model sometimes experiences a singularity. This work bridges the gap between computationally efficient 0D models and 1D models with transport effects. With the improved computational efficiency, the Tanks-in-Series model is promising for parameter estimation, optimization, and battery management systems.

Two papers by Xu *et al.* demonstrate parameter identification for 0D LiS models. The first paper[87] focuses on model selection and a parameter sensitivity study to determine the important parameters to be identified. They started by carrying out a systematic comparison of four different 0D models to the same experimental dataset. All four 0D models are based on ref. 12 and 34 where there is no diffusion or migration terms. The four 0D models differ based on the number of electrochemical reduction reactions, with a range of two reduction reactions to the full set of five reactions to describe the two plateaus. They assumed that all S_8 is dissolved at the start of discharge. Xu *et al.* also carried out a sensitivity analysis by changing one parameter at a time for the full model. Upon comparing the derivative of voltage with respect to the varied parameter, they found that the most significant parameters are the standard potentials, morphology factor (power of the relative porosity), porosity change rate constant, and mass of initial sulfur. The porosity change rate constant is treated as a fitting parameter although it should be a constant relating to density of the precipitated solids. Then, they chose to identify these significant parameters by fitting all four models to experimental data. They concluded that the model with 4 electrochemical reactions (S_4^{2-} is directly reduced to S^{2-}) performs the best in terms of computation time and capturing features well. The full model with 5 reactions does not capture the nucleation dip well. Since it is sufficient to capture features well with a less complicated scheme and with less parameters, Xu *et al.* used this model with 4 reactions in their following paper about online state estimation. We point out that this approach towards sensitivity analysis by varying one parameter at a time is not useful when the base parameters (initial guesses) change as this is a nonlinear model. Bayesian estimation maybe be more useful for parameter estimation.[88]

In this second paper,[89] the focus is on online estimation of the mass of different sulfur species during a discharge. They reformulated the model by converting the system of differential algebraic equations to ordinary differential equations by analytically solving the current equation and writing an

analytical expression for voltage. They found that the model is locally observable. A model is locally observable if the estimated initial states are close to the true value, it is possible to construct an estimator/observer that converges to the true value. They also found that the lowest estimation errors are at the voltage dip while the greatest errors occur at the flat low plateau region. This means that the estimation of parameters is more challenging in the flat region as the voltage is less sensitive to parameters. The largest standard deviation of error is linked to the mass of precipitated Li_2S since the output voltage is not sensitive to mass. Xu *et al.* proposed the use of mass conservation to eliminate two of the seven state variables, mass of solid Li_2S and porosity, and thus improving observability. This can be achieved by assuming that the total sulfur is known and enforcing a mass balance constraint. They used an unscented Kalman filter to perform state estimation during a constant discharge. Based on their results, they recommend that estimation is carried out in two steps: first at the high plateau region using the full model and estimating the total active sulfur mass, then using the reduced model to estimate the low plateau. Xu *et al.* laid out a framework and demonstrated ability to perform online state estimation, showing a viable path for incorporating physics-based models onto BMS for control applications. It is important to note that since this is a 0D model, it will have limited performance at higher rates or if the system is transport-limited.

Conclusions

We reviewed and outlined the advancement of macroscale and microscale continuum modeling literature for lithium–sulfur batteries. Simplified reaction schemes typically employed in lumped models are useful for minimization of parameters while enhancing computational efficiency. Microscale modeling efforts have focused on incorporating insights from experimental methods, such as high-performance liquid chromatography and cyclic voltammetry, to further understand the speciation and the impact of electrolyte engineering. A critical area of research is the reversibility of models. Most models are not able to reproduce all the charging features, and there is still debate about whether the discrepancy is due to missing mechanisms of precipitation phenomena or inaccuracies of the reaction scheme. The presence of multiple phases and mixed speciation within a lithium–sulfur battery means changing conditions throughout a single cycle. Significant progress has been made to model the microscale precipitation within the cathode, and particle-level nucleation and growth mechanisms have been able to capture the rate-dependent dynamics. Experimental efforts have focused on micro and nanostructured cathodes to overcome issues like conductivity, pore clogging, and active material loss due to the high solubility of polysulfides while most models only consider the cathode as a composite material. A microscale model for the cathode has been implemented and considers a mesoporous structure that captures effects of particle size; future modeling work should adopt similarly resolved cathode models. The polysulfide shuttle has been modeled to understand degradation. While lumped macroscale models include shuttling proportional to the current, macroscale modeling of shuttle predicts a more complicated relationship between operating conditions and other limiting phenomena, like transport limitations within the cathode. Lithium metal morphology and reactivity have been approximated by a passivation of the electrochemical active surface with deposition of Li_2S. As cells trend toward lean electrolyte conditions for high energy density, solution phase dynamics become more important due to increased transport limitations. Microscale modeling is key to accurate predictions of speciation and practical operating range; models have focused on areas such as improving experimental agreement for electrolyte resistance and utilizing concentrated solution theory. For scale up and meeting high energy density targets, work has focused on parameters like electrolyte to sulfur and carbon to sulfur ratios for insight into performance under relevant conditions. Electroanalytical methods like EIS and GITT can greatly inform mechanisms and phenomena occurring at different time scales, and the field would benefit from further model development and collaboration in this area. Another important aspect of modeling is alignment of model parameters and predictions to experimental data. Efforts in this area include parameter sensitivities, development of computationally efficient models, and parameter estimation. This research area will become more important as the focus moves from active development (electrolyte engineering, *etc.*) to cell optimization.

Although the progress of continuum models is encouraging and there are many studies that have used experimental data to validate their models, to date, there is no study that utilizes macroscale models to contribute directly to the development of better lithium–sulfur cells. For experimentalists to use modeling insights to engineer better cells, the modeling community should focus on models that closely resemble state-of-the-art high energy density lithium–sulfur cells. This would require alignment of parameters that are physically meaningful and reporting cell-level metrics that are relevant as there is currently a disconnect between model parameters and cell-level design. Also, models that pay attention to details like concentration-dependent electrolyte resistance, concentration solution theory, and transport limitations will be able to model accurate cell performance under low E/S conditions.

Models can guide electrolyte engineering efforts as they can help elucidate reaction schemes through validation with voltage curves but also other electrochemical measurements like CV. However, there is still a fundamental gap that exists due to the inability of existing models to replicate voltage features for both discharging and charging. Possible approaches to resolve this charging challenge are to more thoroughly validate parameters experimentally, understand parallel mechanisms that may allow different pathways during charge *versus* discharge, or include limiting phenomena that a cell undergoes when charging. It is key to recognize that many parameters in LiS modeling have been assumed without proper independent validation. Creative electroanalytical approaches to measuring these key parameters under realistic battery electrolyte conditions is essential, *e.g.*, solubility products. Likewise, continuum

models can be coupled with DFT and AIMD simulations to inform reaction rate constants and conductivities.[2] Only then should the remaining parameters be estimated through fits to experimental data.

Shuttling remains one the major challenges for lithium–sulfur as it is the main cause of irreversible capacity loss. Experimental strategies like coatings, additives, and design of cathode structure can help retain and trap polysulfides in the cathode or preventing passivation on the anode can be informed by modeling. Continuum-scale physics-based models can go beyond describing experimental observations to helping ensure these novel engineering strategies result in quantitatively optimal designs. An important aspect of this optimal design will include more detailed morphological modeling of the lithium anode to improve cycling performance. Note that detailed meso-scale models should also be carefully studied with proper boundary conditions for mass and charge conservation,[90] and numerical mesh/grid convergence studies should be reported to make sure that the results have at least qualitatively converged. As cathode engineering becomes more sophisticated, such as developing micro- and nano-structures for improved conductivity while reducing surface passivation and pore clogging effects, models that move beyond a typical porous composite structure can help understand the evolution of morphology under different conditions and can help optimize engineering designs like particle and pore sizes.

List of symbols

a	Specific surface area of cathode, $m^2\ m^{-3}$
a_0	Initial value of a, $m^2\ m^{-3}$
b	Bruggeman coefficient
$C_{i,\mathrm{ref}}$	Reference concentration of species i, mol m^{-3}
$C_{m,i}$	Concentration of species i in region m, mol m^{-3}
$D_{i,0}$	Diffusion coefficient of species i in the bulk medium, $m^2\ s^{-1}$
D_i	Diffusion coefficient of species i in the porous medium, $m^2\ s^{-1}$
F	Faraday constant, C mol^{-1}
$i_{0,j,\mathrm{ref}}$	Exchange current density of reaction j at reference concentrations, A m^{-2}
i_{app}	Applied current density, A m^{-2}
i_j	Current density from reaction j, A m^{-2}
$i_{m,\mathrm{e}}$	Superficial current density in the electrolyte phase in region m, A m^{-2}
i_{s}	Superficial current density in the solid phase, A m^{-2}
k_k	Rate constant of precipitate k, varying units, see ref. 8
$K_{\mathrm{sp},k}$	Solubility product of precipitate k, varying units, see ref. 8
l_1	Thickness of the cathode, m
l_2	Thickness of the separator, m
$N_{m,i}$	Superficial flux of species i in region m, mol $m^2\ s^{-1}$
n_j	Number of electrons transferred in electrochemical reaction j
R	Gas constant, J $mol^{-1}\ K^{-1}$
r_i	Production rate of species i from electrochemical reactions, mol $m^3\ s^{-1}$
r_i'	Production rate of species i from electrochemical reactions at the interface between the separator and anode, mol $m^{-2}\ s^{-1}$
R_k'	Rate of precipitation of solid species k, mol $m^3\ s^{-1}$
$R_{m,i}$	Production rate of species i due to precipitation reactions in region m, mol $m^3\ s^{-1}$
$s_{\mathrm{a},j}$	Stoichiometric coefficient of anodic species in electrochemical j
$s_{\mathrm{c},j}$	Stoichiometric coefficient of cathodic species in electrochemical j
$s_{i,j}$	Stoichiometric coefficient of species i in electrochemical reaction j
T	Temperature, K
t	Time, s
U_j^θ	Standard open circuit potential (OCP) of electrochemical reaction j, V
$U_{j,\mathrm{ref}}$	OCP of electrochemical reaction j at reference concentrations, V
$\tilde{V}_k$	Molar volume of the precipitate k, $m^3\ mol^{-1}$
Z_i	Charge number of species i

Greek symbols

$\alpha_{\mathrm{a},j}$	Anodic transfer coefficient of reaction j
$\alpha_{\mathrm{c},j}$	Cathodic transfer coefficient of reaction j
$\gamma_{i,k}$	Number of ionic species i produced by the dissociation of precipitate k
ε_m	Porosity of region m
$\varepsilon_{m,k}$	Volume fraction of precipitate k in region m
η_j	Overpotential for electrochemical reaction j
ξ	Morphology parameter
σ	Effective conductivity of solid phase of the cathode, S m^{-1}
$\phi_{m,\mathrm{e}}$	Potential in the liquid phase in region m, V
ϕ_{s}	Potential in the solid phase, V

Conflicts of interest

The authors have no conflicts of interest to declare.

Acknowledgements

The authors would like to thank the Assistant Secretary for Energy Efficiency and Renewable Energy, Office of Vehicle Technologies of the U.S. Department of Energy through the Advanced Battery Materials Research (BMR) Program (Battery500 Consortium) for funding support of this work. We acknowledge support provided by the Boeing-Sutter endowment and Clean Energy Institute at the University of Washington.

References

1 T. Cleaver, P. Kovacik, M. Marinescu, T. Zhang and G. Offer, *J. Electrochem. Soc.*, 2018, **165**, A6029–A6033.
2 Z. Liu, A. Mistry and P. P. Mukherjee, *J. Electrochem. Energy Convers. Storage*, 2018, **15**, 010802.

3 Y. Diao, K. Xie, S. Xiong and X. Hong, *J. Power Sources*, 2013, **235**, 181–186.
4 S. Li, M. Jiang, Y. Xie, H. Xu, J. Jia and J. Li, *Adv. Mater.*, 2018, **30**, 1706375.
5 A. Bhargav, J. He, A. Gupta and A. Manthiram, *Joule*, 2020, **4**, 285–291.
6 R. Fang, S. Zhao, Z. Sun, D.-W. Wang, H.-M. Cheng and F. Li, *Adv. Mater.*, 2017, **29**, 1606823.
7 J. Brückner, S. Thieme, H. T. Grossmann, S. Dörfler, H. Althues and S. Kaskel, *J. Power Sources*, 2014, **268**, 82–87.
8 K. Kumaresan, Y. Mikhaylik and R. E. White, *J. Electrochem. Soc.*, 2008, **155**, A576–A582.
9 A. N. Mistry and P. P. Mukherjee, *J. Phys. Chem. C*, 2018, **122**, 23845–23851.
10 Y. V. Mikhaylik and J. R. Akridge, *J. Electrochem. Soc.*, 2004, **151**, A1969–A1976.
11 T. Danner, G. Zhu, A. F. Hofmann and A. Latz, *Electrochim. Acta*, 2015, **184**, 124–133.
12 M. Marinescu, T. Zhang and G. J. Offer, *Phys. Chem. Chem. Phys.*, 2016, **18**, 584–593.
13 N. Erisen and D. Eroglu, *Int. J. Energy Res.*, 2020, **44**, 10599–10611.
14 T. Zhang, M. Marinescu, S. Walus and G. J. Offer, *Electrochim. Acta*, 2016, **219**, 502–508.
15 S. Waluś, C. Barchasz, R. Bouchet, J.-C. Leprêtre, J.-F. Colin, J.-F. Martin, E. Elkaïm, C. Baehtz and F. Alloin, *Adv. Energy Mater.*, 2015, **5**, 1500165.
16 Y. Gorlin, M. U. M. Patel, A. Freiberg, Q. He, M. Piana, M. Tromp and H. A. Gasteiger, *J. Electrochem. Soc.*, 2016, **163**, A930–A939.
17 S. Drvarič Talian, J. Moškon, R. Dominko and M. Gaberščček, *ACS Appl. Mater. Interfaces*, 2017, **9**, 29760–29770.
18 C. Barchasz, F. Molton, C. Duboc, J.-C. Leprêtre, S. Patoux and F. Alloin, *Anal. Chem.*, 2012, **84**, 3973–3980.
19 P. Schön, F. Hintz and U. Krewer, *Electrochim. Acta*, 2019, **295**, 926–933.
20 P. Schön and U. Krewer, *Electrochim. Acta*, 2021, **373**, 137523.
21 Y.-C. Lu, Q. He and H. A. Gasteiger, *J. Phys. Chem. C*, 2014, **118**, 5733–5741.
22 V. Thangavel, A. Mastouri, C. Guéry, M. Morcrette and A. A. Franco, *Batteries Supercaps*, 2021, **4**, 152–162.
23 M. Safari, C. Y. Kwok and L. F. Nazar, *ACS Cent. Sci.*, 2016, **2**, 560–568.
24 J. Shim, T. J. Ko and K. Yoo, *J. Ind. Eng. Chem.*, 2019, **80**, 283–291.
25 A. Gupta, A. Bhargav and A. Manthiram, *Adv. Energy Mater.*, 2019, **9**, 1803096.
26 C. D. Parke, A. Subramaniam, V. R. Subramanian and D. T. Schwartz, *ChemElectroChem*, 2021, **8**, 1098–1106.
27 T. A. Pascal, K. H. Wujcik, D. R. Wang, N. P. Balsara and D. Prendergast, *Phys. Chem. Chem. Phys.*, 2017, **19**, 1441–1448.
28 E. P. Kamphaus and P. B. Balbuena, *J. Phys. Chem. C*, 2017, **121**, 21105–21117.
29 M. Ghaznavi and P. Chen, *J. Power Sources*, 2014, **257**, 402–411.
30 M. Ghaznavi and P. Chen, *Electrochim. Acta*, 2014, **137**, 575–585.
31 T. Danner and A. Latz, *Electrochim. Acta*, 2019, **322**, 134719.
32 C. Park, A. Ronneburg, S. Risse, M. Ballauff, M. Kanduč and J. Dzubiella, *J. Phys. Chem. C*, 2019, **123**, 10167–10177.
33 M. R. Busche, P. Adelhelm, H. Sommer, H. Schneider, K. Leitner and J. Janek, *J. Power Sources*, 2014, **259**, 289–299.
34 T. Zhang, M. Marinescu, L. O'Neill, M. Wild and G. Offer, *Phys. Chem. Chem. Phys.*, 2015, **17**, 22581–22586.
35 K. Yoo, M.-K. Song, E. J. Cairns and P. Dutta, *Electrochim. Acta*, 2016, **213**, 174–185.
36 T. Zhang, M. Marinescu, S. Walus, P. Kovacik and G. J. Offer, *J. Electrochem. Soc.*, 2018, **165**, A6001–A6004.
37 C. Xiong, T. S. Zhao, Y. X. Ren, H. R. Jiang and X. L. Zhou, *Electrochim. Acta*, 2019, **296**, 954–963.
38 Y. X. Ren, T. S. Zhao, M. Liu, P. Tan and Y. K. Zeng, *J. Power Sources*, 2016, **336**, 115–125.
39 P. Andrei, C. Shen and J. P. Zheng, *Electrochim. Acta*, 2018, **284**, 469–484.
40 H.-J. Peng, J.-Q. Huang, X.-Y. Liu, X.-B. Cheng, W.-T. Xu, C.-Z. Zhao, F. Wei and Q. Zhang, *J. Am. Chem. Soc.*, 2017, **139**, 8458–8466.
41 S.-H. Yu, X. Huang, K. Schwarz, R. Huang, T. A. Arias, J. D. Brock and H. D. Abruña, *Energy Environ. Sci.*, 2018, **11**, 202–210.
42 F. Y. Fan and Y.-M. Chiang, *J. Electrochem. Soc.*, 2017, **164**, A917–A922.
43 A. Mistry and P. P. Mukherjee, *J. Phys. Chem. C*, 2017, **121**, 26256–26264.
44 K. Shah, A. Subramaniam, L. Mishra, T. Jang, M. Z. Bazant, R. D. Braatz and V. R. Subramanian, *J. Electrochem. Soc.*, 2020, **167**, 133501.
45 Z. Liu, D. Hubble, P. B. Balbuena and P. P. Mukherjee, *Phys. Chem. Chem. Phys.*, 2015, **17**, 9032–9039.
46 Z. W. Seh, W. Li, J. J. Cha, G. Zheng, Y. Yang, M. T. McDowell, P.-C. Hsu and Y. Cui, *Nat. Commun.*, 2013, **4**, 1331.
47 X. Ji, S. Evers, R. Black and L. F. Nazar, *Nat. Commun.*, 2011, **2**, 325.
48 V. Thangavel, K.-H. Xue, Y. Mammeri, M. Quiroga, A. Mastouri, C. Guéry, P. Johansson, M. Morcrette and A. A. Franco, *J. Electrochem. Soc.*, 2016, **163**, A2817–A2829.
49 N. Jayaprakash, J. Shen, S. S. Moganty, A. Corona and L. A. Archer, *Angew. Chem., Int. Ed.*, 2011, **50**, 5904–5908.
50 J. Shim, K. A. Striebel and E. J. Cairns, *J. Electrochem. Soc.*, 2002, **149**, A1321–A1325.
51 S.-E. Cheon, K.-S. Ko, J.-H. Cho, S.-W. Kim, E.-Y. Chin and H.-T. Kim, *J. Electrochem. Soc.*, 2003, **150**, A796–A799.
52 J. Zhao, Y. Yang, R. S. Katiyar and Z. Chen, *J. Mater. Chem. A*, 2016, **4**, 6124–6130.
53 C. Monroe and J. Newman, *J. Electrochem. Soc.*, 2005, **152**, A396–A404.
54 P. Barai, K. Higa and V. Srinivasan, *J. Electrochem. Soc.*, 2018, **165**, A2654–A2666.
55 P. Bai, J. Guo, M. Wang, A. Kushima, L. Su, J. Li, F. R. Brushett and M. Z. Bazant, *Joule*, 2018, **2**, 2434–2449.

56 K. N. Wood, E. Kazyak, A. F. Chadwick, K.-H. Chen, J.-G. Zhang, K. Thornton and N. P. Dasgupta, *ACS Cent. Sci.*, 2016, **2**, 790–801.
57 A. Subramaniam, J. Chen, T. Jang, N. R. Geise, R. M. Kasse, M. F. Toney and V. R. Subramanian, *J. Electrochem. Soc.*, 2019, **166**, A3806–A3819.
58 X. Chen, T.-Z. Hou, B. Li, C. Yan, L. Zhu, C. Guan, X.-B. Cheng, H.-J. Peng, J.-Q. Huang and Q. Zhang, *Energy Storage Mater.*, 2017, **8**, 194–201.
59 Z. Liu, S. Bertolini, P. B. Balbuena and P. P. Mukherjee, *ACS Appl. Mater. Interfaces*, 2016, **8**, 4700–4708.
60 M. Marinescu, L. O'Neill, T. Zhang, S. Walus, T. E. Wilson and G. J. Offer, *J. Electrochem. Soc.*, 2018, **165**, A6107–A6118.
61 A. F. Hofmann, D. N. Fronczek and W. G. Bessler, *J. Power Sources*, 2014, **259**, 300–310.
62 J.-W. Choi, J.-K. Kim, G. Cheruvally, J.-H. Ahn, H.-J. Ahn and K.-W. Kim, *Electrochim. Acta*, 2007, **52**, 2075–2082.
63 N. Kamyab, P. T. Coman, S. K. Madi Reddy, S. Santhanagopalan and R. E. White, *J. Electrochem. Soc.*, 2020, **167**, 130532.
64 S. M. Al-Mahmoud, J. W. Dibden, J. R. Owen, G. Denuault and N. Garcia-Araez, *J. Power Sources*, 2016, **306**, 323–328.
65 D. Moy, A. Manivannan and S. R. Narayanan, *J. Electrochem. Soc.*, 2015, **162**, A1–A7.
66 G. Wen, S. Rehman, T. G. Tranter, D. Ghosh, Z. Chen, J. T. Gostick and M. A. Pope, *Chem. Mater.*, 2020, **32**, 4518–4526.
67 A. N. Mistry and P. P. Mukherjee, *J. Phys. Chem. C*, 2018, **122**, 18329–18335.
68 G. L. Shebert, S. Zamani, C. Yi and Y. L. Joo, *J. Mater. Chem. A*, 2020, **8**, 4341–4353.
69 K. Zhu, C. Wang, Z. Chi, F. Ke, Y. Yang, A. Wang, W. Wang and L. Miao, *Front. Energy Res.*, 2019, **7**, 123.
70 J. Liu, Z. Bao, Y. Cui, E. J. Dufek, J. B. Goodenough, P. Khalifah, Q. Li, B. Y. Liaw, P. Liu, A. Manthiram, Y. S. Meng, V. R. Subramanian, M. F. Toney, V. V. Viswanathan, M. S. Whittingham, J. Xiao, W. Xu, J. Yang, X.-Q. Yang and J.-G. Zhang, *Nat. Energy*, 2019, **4**, 180–186.
71 N. Erisen, N. B. Emerce, S. C. Erensoy and D. Eroglu, *Int. J. Energy Res.*, 2018, **42**, 2631–2642.
72 C. Michaelis, N. Erisen, D. Eroglu and G. M. Koenig, *Int. J. Energy Res.*, 2019, **43**, 874–883.
73 N. B. Emerce and D. Eroglu, *J. Electrochem. Soc.*, 2019, **166**, A1490–A1500.
74 H. M. Bilal and D. Eroglu, *J. Electrochem. Soc.*, 2021, **168**, 030502.
75 B. D. McCloskey, *J. Phys. Chem. Lett.*, 2015, **6**, 4581–4588.
76 J.-J. Kim, H. S. Kim, J. Ahn, K. J. Lee, W. C. Yoo and Y.-E. Sung, *J. Power Sources*, 2016, **306**, 617–622.
77 U. Košir, I. Kralj Cigić, J. Markelj, S. Drvarič Talian and R. Dominko, *Electrochim. Acta*, 2020, **363**, 137227.
78 Y. Zhao, J. Zhang and J. Guo, *ACS Appl. Mater. Interfaces*, 2021, **13**, 31749–31755.
79 J. W. Dibden, N. Meddings, J. R. Owen and N. Garcia-Araez, *ChemElectroChem*, 2018, **5**, 445–454.
80 J. H. Lee, J. Kang, S.-W. Kim, W. Halim, M. W. Frey and Y. L. Joo, *ACS Omega*, 2018, **3**, 16465–16471.
81 Z. Deng, Z. Zhang, Y. Lai, J. Liu, J. Li and Y. Liu, *J. Electrochem. Soc.*, 2013, **160**, A553–A558.
82 X. Qiu, Q. Hua, L. Zheng and Z. Dai, *RSC Adv.*, 2020, **10**, 5283–5293.
83 S. Waluś, C. Barchasz, R. Bouchet and F. Alloin, *Electrochim. Acta*, 2020, **359**, 136944.
84 D. N. Fronczek and W. G. Bessler, *J. Power Sources*, 2013, **244**, 183–188.
85 M. Ghaznavi and P. Chen, *J. Power Sources*, 2014, **257**, 394–401.
86 C. D. Parke, A. Subramaniam, S. Kolluri, D. T. Schwartz and V. R. Subramanian, *J. Electrochem. Soc.*, 2020, **167**, 163503.
87 C. Xu, T. Cleary, G. Li, D. Wang and H. Fathy, *ASME Lett. Dyn. Syst. Control*, 2021, **1**, 041001.
88 V. Ramadesigan, K. Chen, N. A. Burns, V. Boovaragavan, R. D. Braatz and V. R. Subramanian, *J. Electrochem. Soc.*, 2011, **158**, A1048–A1054.
89 C. Xu, T. Cleary, D. Wang, G. Li, C. Rahn, D. Wang, R. Rajamani and H. K. Fathy, *J. Power Sources*, 2021, **489**, 229495.
90 L. Mishra, A. Subramaniam, T. Jang, K. Shah, M. Uppaluri, S. A. Roberts and V. R. Subramanian, *J. Electrochem. Soc.*, 2021, **168**, 092502.

